

Analysis, Design and Implementation of a Static Conductance-Based MPPT Method

Oswaldo Lopez-Santos* *Senior Member, IEEE*, Germain Garcia, Luis Martinez-Salamero, *Senior Member, IEEE*, Roberto Giral *Senior Member*, Enric Vidal-Idiarte *Member, IEEE*, Maria Camila Merchan-Riveros, *Student Member, IEEE*, and Yamel Moreno-Guzman

Abstract

This paper introduces a maximum power point tracking (MPPT) method based on a power (P) versus static conductance (G) curve of a photovoltaic (PV) array. The maximum power point (MPP) is tracked by comparing the PV array instantaneous power to a varying power reference generated by the MPPT algorithm. The comparison error is used to reduce or increase the conductance at which the PV array is forced to operate until the MPP is reached. Simultaneously, the error is used to change the power reference until the trajectory of this reference in the P-G curve enters a limit cycle around the MPP.

The P-G curve is derived from a piecewise linear approximation of the current versus voltage (I-V) curve, which facilitates the analytical description of the tracking operation.

The technique reported can also be implemented by means of simple analog or digital circuitry and requires two sensors to measure the instantaneous PV array current and voltage. It uses only four tuning parameters, which are selected depending on the maximum value of the derivative of the power with respect to the conductance.

The theoretical predictions are verified with simulations and experimental results. The latter show that the procedure performs well enough to be favorably compared with the most efficient MPPT methods.

Index Terms

Maximum power point tracking, P-G curve, extremum-seeking control, photovoltaic generators

* Corresponding author.

I. INTRODUCTION

Of the various control functions in photovoltaic (PV) systems, the controller processing the instantaneous power extracted from the PV modules is one that most influences the overall performance of the system. This controller not only makes the system work at the maximum power point (MPP) but also permanently tracks it when unpredictable changes appear in the environmental variables (irradiance and temperature). This justifies the use of tracking algorithms or optimization methods to obtain “Maximum Power Point Tracking” (MPPT), which have been extensively studied and compared in the literature [1]-[9]. The impact of the MPPT on photovoltaic applications is crucial when modular solutions with a limited number of solar panels are used as alternatives to centralized installations. This is largely because the power extracted can be disaggregated, which makes it possible to use a dedicated MPPT for each PV module and reduce the consequences of partial shadowing.

The numerous existing MPPT methods are classified as either parametric-based or heuristic-based methods [10]-[12]. The parametric-based methods use a parametric model and measure the PV module parameters directly or indirectly. The heuristic-based methods measure the electric variables to determine whether the system is at the maximum power point. In historical terms, the heuristic MPPT methods can be classified as one of the Extremum Seeking Control (ESC) techniques, which have been studied since the 1950s. One group of these techniques uses algorithms that apply an additive disturbance or an oscillation to one or more variables and then observe the evolution of the system and determine the appropriate control action. The disturbance can be applied to either the electric variables (current and voltage) or the control variables such as the frequency [13]-[15] or duty cycle [16]-[18]. This method, known as Perturb and Observe (P&O), is widely used because of its simplicity and low cost [19]-[24]. However, its performance depends on the amplitude and time latency of the perturbations introduced, which is a considerable limitation. A second group uses algorithms that apply slope regulation because if a function is to reach its maximum value a null derivative must be detected. These algorithms also introduce a disturbance into the system so that the derivative of the power can be evaluated and the control action determined. Some of the methods in this second group are Incremental Conductance (INC) and Incremental Resistance [25]-[30]. However, the need for these algorithms to compute derivatives means that they are limited by the presence of noise and singularities in the numerical operations. A third group uses algorithms that work with an error signal between

the maximum or a fictitious maximum and the actual operational point in order to impose a trajectory toward the real maximum of the function. These algorithms are called peak-holding, peak-searching or peak-detection and are widely applied in many areas of engineering. This group includes fuzzy-logic [31]-[34], predictive [35] and random search methods [36]. Other methods such as Ripple Correlation Control (RPC) can be regarded as ESC methods [37] because they use a natural oscillatory component and the knowledge of its behavior around the optimum of the function to drive the system to the desired operational point [38]-[39]. ESC includes many different methods [40]-[44], some of which use a sliding-mode (SM) strategy to ensure that the maximum is reached. These MPPT techniques are known in the literature as Sliding-Mode Extremum Seeking Control (SM-ESC) methods [45]-[49] and, among other advantages, perform well and are easily integrated with the control of the DC-DC power converters. It is also worth mentioning that the estimation algorithm of the maximum power point reported in [50] does not need to track the point because it identifies in real time the complete current-voltage characteristics of the panel from the measurements of six voltage and current coordinates near the operating point.

The latest advances and contributions in the field of MPPT focus on the problem of partial shadowing, which involves multiple maximum points in the power vs. voltage (P-V) characteristic, which transforms the problem into the tracking of the global MPP [51]-[54]. Nevertheless, all those solutions that improve existing ones or develop new ways to track a single MPP continue to be the object of interest in research into photovoltaic generation [55]-[61]. Current efforts focus on the rapidity, robustness, simplicity and feasibility of these new solutions, only a few of which can be implemented with both analogue and digital electronic circuitry.

Most of the MPPT methods mentioned use power versus voltage or power versus current curves to explain their corresponding algorithms. The output of the algorithms reduces or increases the value of the voltage or the current at which the PV generator is forced to operate. The decision is often illustrated by the resulting trajectory of the PV generator operating point along these curves. One example of this is the Incremental Conductance (INC) approach, which is based on the fact that the slope of the PV generator power curve (i.e. power versus voltage or power versus current) is zero at MPP, positive on the left and negative on the right. The MPP is tracked by comparing the instantaneous conductance of the PV generator to the incremental conductance so that the voltage at which the PV array is forced to operate in a power versus voltage curve decreases or increases depending on the result of the comparison. The behavior is similar in a power versus current curve when the value of the current at which the PV is forced to operate is changed. Two

sensors are required to measure the instantaneous PV generator current and voltage, and a DSP or a microcontroller to implement the algorithm which explicitly uses derivatives and divisions.

The work reported here presents an MPPT method that explains tracking with a power (P) versus static conductance (G) curve of a solar array. The algorithm generates a varying power reference, which is compared with the PV array instantaneous power. The comparison error is processed to change the operating point of the array by modifying its static conductance until the MPP is reached. The error is used simultaneously to alter the power reference until the trajectory of the latter in the P-G curve attains a rhomboidal limit cycle around the MPP. The technique proposed can be categorized as ESC because it internally generates the oscillating signals required to bring the system to its MPP.

A piecewise linear approximation of the current versus voltage (I-V) curve of the PV array is used to derive the P-G curve, which eventually facilitates the analytical description of the tracking operation.

The technique proposed can also be implemented analogically or digitally. These implementations require the instantaneous measurement of the current and voltage of the PV array. Neither derivatives nor divisions are used.

The method is illustrated by matching the static conductance of a PV generator and the static input conductance of a quadratic boost converter that constitutes the first stage of a solar microinverter. The quadratic boost converter transfers the energy from the PV generator to a 400 DC regulated bus that eventually supplies a grid-connected full-bridge inverter.

The conductance is matched by imposing loss-free-resistor behavior on the quadratic boost converter by means of sliding-mode control [62]-[64]. The resulting static input conductance of the quadratic boost converter relates the input voltage and input current on the switching surface used in the sliding-mode control. The value of this conductance is the MPP conductance and is provided by the proposed MPPT. Figs 1a, 1b, and 1c illustrate the main ideas involved in the conductance matching. The regulation scheme is based on a two-loop control approach, in which the inner loop uses a sliding-mode strategy to impose proportionality between the input voltage and input current in the quadratic boost converter. The outer loop is based on the MPPT, which uses the measured voltage and current values of the PV array to generate the appropriate value of the static conductance required by the inner loop. The goal of the outer loop is to provide the optimal value of G (G_{opt}) that will result in the intersection of the I-V curve of the PV array and the curve of the DC characteristics of the converter input port (see Fig.1b). Since the converter is a two-port POPI (DC input power equal to DC output power) [65], the power absorbed at the converted input port will be transferred to the DC link at the output port (see Fig. 1c), where the

resulting operating point in the DC bus is the intersection of the hyperbola corresponding to the absorbed power and the vertical straight line representing the constant voltage of the DC link.

The rest of the paper is organized as follows: Section II states the problem and introduces the MPPT algorithm, which is analyzed in detail in section III. In particular, a stability analysis yields the main conditions the algorithm parameters must satisfy. These conditions involve the maximum of the slope of the P-G characteristic, which is evaluated in section III. In section IV, the sliding-mode LFR control applied to the DC-DC converter is briefly recalled and used in section V to validate the proposed MPPT algorithm by means of simulation and experiment. Subsequently, the proposed method is compared with other methods in section VI. Finally, the conclusions are summarized in section VII.

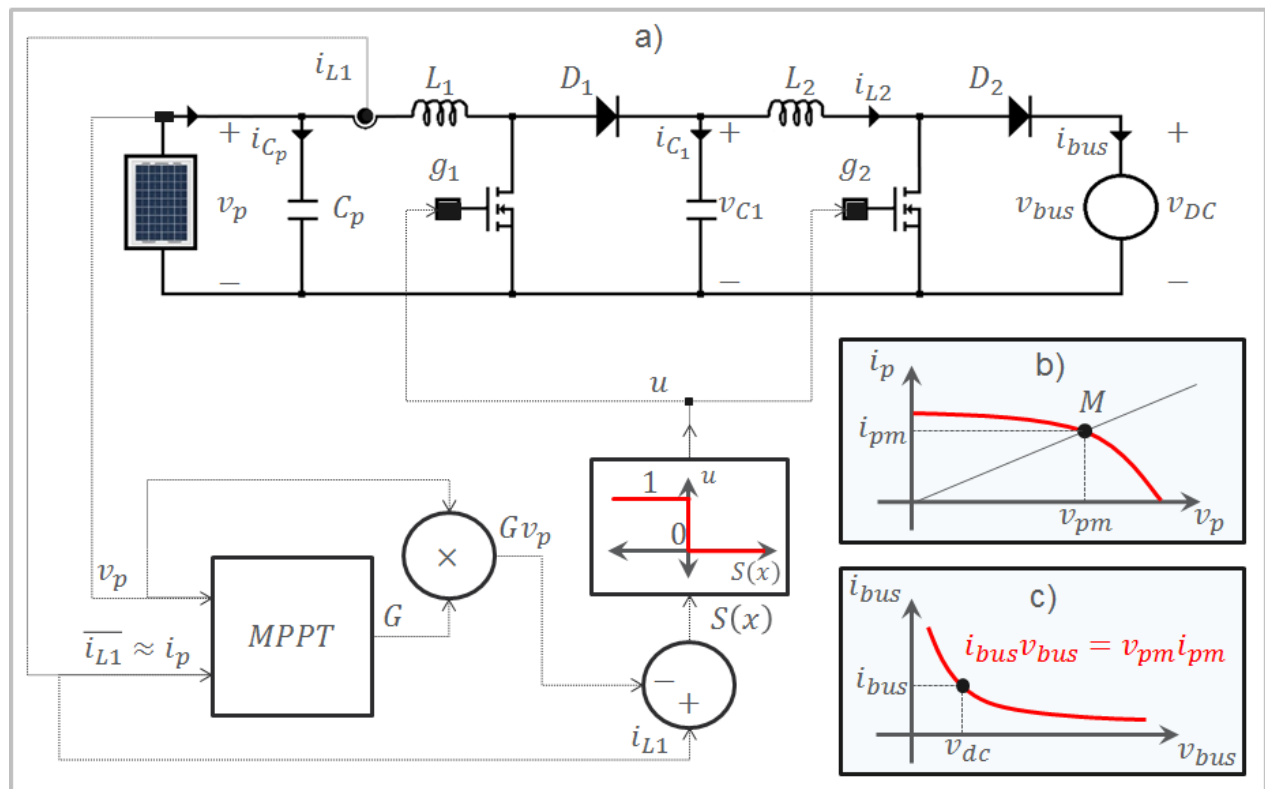


Fig. 1. (a) Block diagram illustrating the impedance matching of a PV array and a regulated DC bus using a quadratic boost converter as power interface. (b) Intersection of PV array and converter characteristics at MPP (Point M). (c) Operating point of the regulated DC bus.

II. PROBLEM STATEMENT

The current or the power delivered by a PV module can be modeled as a function of the output voltage as shown in Fig. 2. For a given PV module, it can be observed that different I-V and P-V

curves (four in Fig. 2) can be obtained, each one of which corresponds to an irradiance level. In this context v_{mpp} denotes the voltage of the PV module at the MPP of the P-V characteristic, and the corresponding current is $i_{p_{mpp}}$. These two characteristic curves are considered by most MPPT methods and can be used to derive geometrical approximations that facilitate the mathematical analysis [66]. The MPP for a given irradiance level E_p also has a corresponding conductance value at the MPP (G_{mpp}) which can be derived from the relation between the current and voltage of the PV module at the MPP. Hence, the MPPT problem can also be solved if the input conductance of the power converter is forced to be equal to the conductance of the PV module at the MPP.

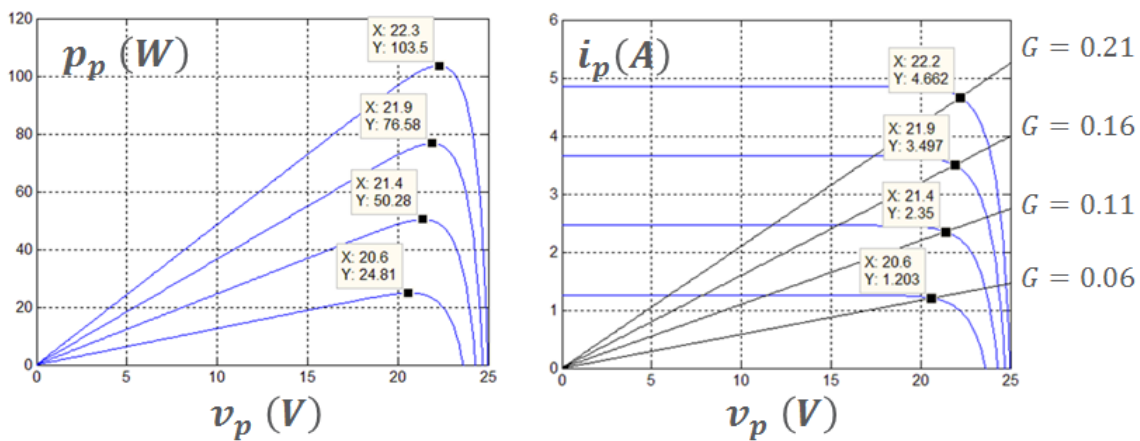


Fig. 2. I-V and P-V characteristics of a PV module

Considering the above remarks, the MPP can be tracked using the P-G characteristic of the PV module. As can be easily demonstrated, the P-G characteristic can be ideally defined for all positive values of conductance between zero and infinity.

The panel voltage range extends from zero (short-circuit) to open-circuit voltage. However, the practical range can be limited by the presence of the DC-DC switching converter matching the panel and the load. The limitation is apparent when the matching operation is modelled by a DC-DC transformer whose transformer ratio is the converter static gain, i.e. a function of the duty cycle. This situation appears when the MPPT is based on a power (P) versus voltage (V) PV curve, which is used to modify the duty cycle in order to eventually change the operating point of the panel. In the case considered here, the load is a 400 V DC regulated bus that would impose a limited excursion of the duty cycle, and therefore of the input voltage, if a DC-DC transformer-based approach was used.

In the proposed method, the limits of the panel voltage range are represented by a zero value of the conductance (open-circuit voltage) and an infinite value of the conductance (short-circuit) in the power (P) versus static conductance (G) curve. However, the DC-DC switching converter doesn't limit the excursion between the extreme points of the range. This is because the converter matching operation is modelled by a loss-free resistor (LFR), i.e. the converter input port can be emulated by a resistor whose conductance can take any value between zero and infinite. Besides, the LFR exhibits a nature of power source at the converter output port, the output power being the power absorbed by the emulated resistor at the input port. Therefore, the 400 V DC regulated bus absorbs the current supplied by the power source for any value of the voltage panel between zero and the open-circuit voltage.

The proposed MPPT uses conductance G as the manipulated variable to force the input conductance of a DC-DC converter to be equal to the conductance of the PV module at the maximum power point (G_{mpp}). Because of the variable structure nature of the proposed MPPT, the instantaneous power of the PV module $P_p(t)$ is forced to remain in the neighborhood of the average value of an internal power reference $P_{p_{ref}}(t)$ which permanently tracks the MPP. Note that $P_p(t)$ is the real power delivered by the panel while $P_{p_{ref}}(t)$ is an auxiliary variable created by the control algorithm to track the MPP.

III. PROPOSED MPPT METHOD

The proposed MPPT method has two fundamental objectives: 1) To eliminate the error $\varepsilon(t) = P_{p_{ref}}(t) - P_p(t)$ thus ensuring that the internal power reference $P_{p_{ref}}(t)$ is tracked, and 2) To guarantee that the reference $P_{p_{ref}}(t)$ increases automatically until it reaches the maximal power P_{mp} where it is maintained. These objectives can be achieved by modifying the conductance $G(t)$ (see Fig. 3).

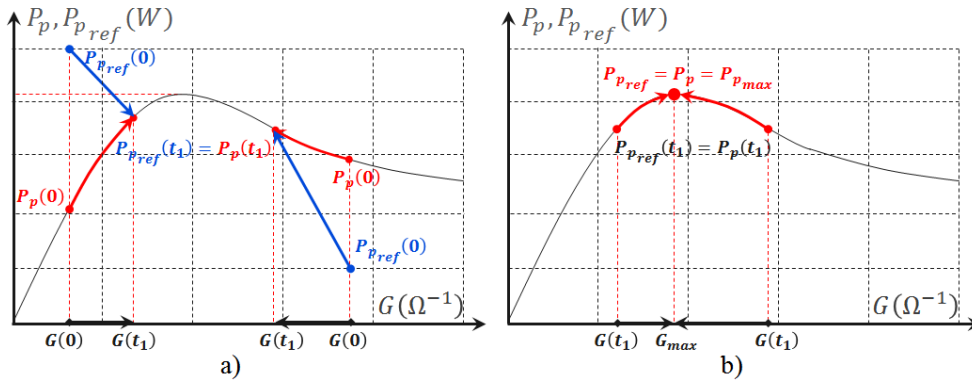


Fig. 3. Trajectories of the two objectives of the MPPT on the P-G plane

Fig. 3a considers two cases of initialization: i.e., to the left and to the right of the MPP. In both situations, the real power tracks the internal reference and both signals reach the maximum value (see Fig. 3b).

In addition, when there is an abrupt change in irradiance, a discontinuous change in $P_p(t)$ is observed and the reference $P_{p_ref}(t)$ must be automatically redefined so that it converges on the new MPP. A block diagram representing the proposed MPPT is given in Fig. 4. The block diagram is structurally identical to the one reported in [67], the first paper to discuss self-optimization based on sliding-mode control. However, in our proposal the nonlinear functions of the error $u(\varepsilon)$ and $v(\varepsilon)$ are different, and the panel is characterized by the power versus conductance characteristics instead by the power versus converter duty cycle. As a result, no sliding-motions are induced in the proposal but the complete resulting dynamics can be explained analytically and therefore the criteria for MPPT parameter selection are clearly derived.

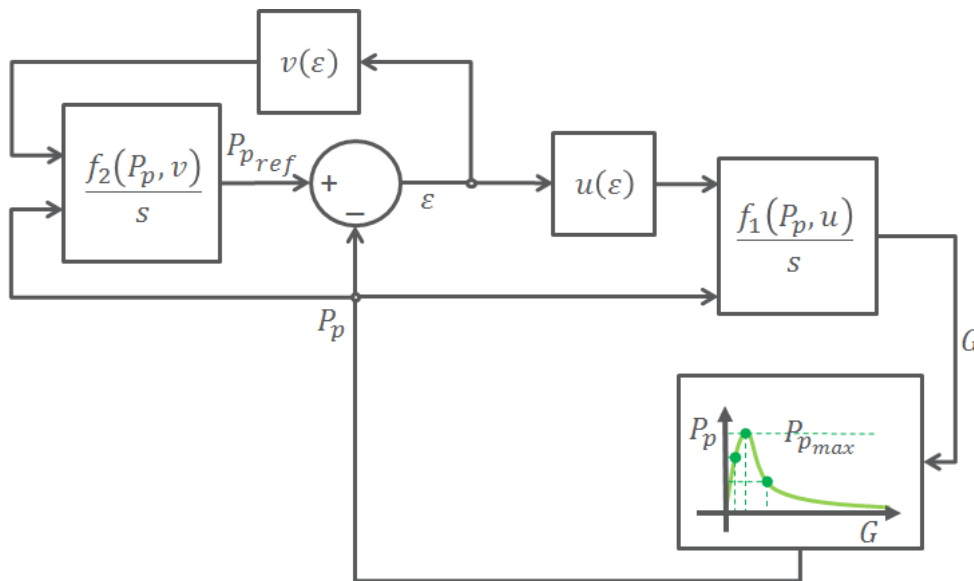


Fig. 4. Block diagram of the proposed self-optimized MPPT algorithm based on P-G characteristics

The algorithm uses the instantaneous value of the panel power $P_p(t)$, which is obtained from the current and voltage measurements in the PV panel. The MPPT also uses the error ε relating $P_p(t)$ and the auxiliary variable $P_{p_{ref}}(t)$.

The PV operating point, and hence $P_p(t)$, is changed by modifying the static conductance G of the panel. This conductance is a triangular signal with positive slope when G increases and with negative slope when G decreases. Note that G is a triangular signal because it is the integral of a square waveform whose levels are given by either $+P_p$ or $-P_p$, depending on the sign of ε .

$P_{p_{ref}}(t)$ is also a triangular signal because it is the integral of a square waveform whose levels can be $+K_2P_p$ or $-(M - K_2)P_p$, with $M > K_2$, depending on the sign of ε . As shown in the next subsection and Appendix I, the error ε tends to zero in finite time, this resulting in an equilibrium point wherein the panel power corresponds to MPP, i.e., $P_p(t) = P_{max}$, while $P_{p_{ref}}(t)$ equals $P_p(t)$. However, when the nonlinear function $v(\varepsilon)$ is modified by the insertion of a hysteresis band, it is the average value of $P_{p_{ref}}(t)$ which equals $P_p(t) = P_{max}$ in the equilibrium point as demonstrated in subsection B.

The equations associated with the block diagram above can be expressed as:

$$\frac{dG}{dt} = f_1(P_p, u) \quad (1)$$

$$\frac{dP_{p_{ref}}}{dt} = f_2(P_p, v) \quad (2)$$

$$f_1(P_p, u) = K_1 P_p u, \quad K_1 > 0 \quad (3)$$

$$f_2(P_p, v) = K_2 P_p + M P_p v, \quad K_2 > 0, \quad M > 0 \quad (4)$$

$$\varepsilon(t) = P_{p_{ref}}(t) - P_p(t) \quad (5)$$

$$u = \text{sign}(\varepsilon) \quad (6)$$

$$v = -\frac{1}{2} - \frac{1}{2} \text{sign}(\varepsilon) \quad (7)$$

The functions u and v are represented in Fig. 5.

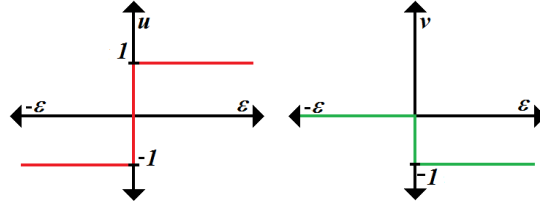


Fig. 5. Ideal switching functions of the proposed MPPT.

A) Regulation for $\varepsilon = 0$.

First, the conditions for the stability of the regulation law $P_p = P_{p_{ref}}$ are analyzed. This requires that the conditions constants M, K_1 and K_2 must satisfy to guarantee a zero regulation error be determined. Consider the quadratic Lyapunov function:

$$V(\varepsilon) = \frac{1}{2} \varepsilon^2 \quad (8)$$

Stability is ensured if $\frac{dV}{dt} = \varepsilon \dot{\varepsilon} < 0$. Therefore,

$$\varepsilon \dot{\varepsilon} = \varepsilon P_p \left[-\frac{1}{2} M - \frac{1}{2} M \text{sign}(\varepsilon) + K_2 - \frac{dP_p}{dG} K_1 \text{sign}(\varepsilon) \right] \quad (9)$$

But $\varepsilon = |\varepsilon| \text{sign}(\varepsilon)$ and $|\varepsilon| = \varepsilon \cdot \text{sign}(\varepsilon)$. Then:

$$\begin{aligned} \varepsilon \dot{\varepsilon} &= P_p \left[-\frac{1}{2} M \varepsilon - \frac{1}{2} M |\varepsilon| + K_2 \varepsilon - \frac{dP_p}{dG} K_1 |\varepsilon| \right] \\ &= |\varepsilon| P_p \left[-\frac{1}{2} M \text{sign}(\varepsilon) - \frac{1}{2} M + K_2 \text{sign}(\varepsilon) - \frac{dP_p}{dG} K_1 \right] \end{aligned} \quad (10)$$

1) If $\varepsilon > 0$:

$$\varepsilon \dot{\varepsilon} = |\varepsilon| P_p \left[-M + K_2 - \frac{dP_p}{dG} K_1 \right] \quad (11)$$

$$\text{If } M > K_2 + \left| \frac{dP_p}{dG} \right|_{max} K_1 \text{ then } M > K_2 - \frac{dP_p}{dG} K_1 \text{ and } \varepsilon \dot{\varepsilon} < 0 \quad (12)$$

2) If $\varepsilon < 0$

$$\varepsilon \dot{\varepsilon} = |\varepsilon| P_p \left[-K_2 - \frac{dP_p}{dG} K_1 \right] \quad (13)$$

$$\text{If } K_2 > \left| \frac{dP_p}{dG} \right|_{max} K_1 \text{ then } K_2 > -\frac{dP_p}{dG} K_1 \text{ and } \varepsilon \dot{\varepsilon} < 0 \quad (14)$$

In conclusion, the conditions for guaranteeing $\varepsilon \dot{\varepsilon} < 0$ are:

$$M > K_2 + \left| \frac{dP_p}{dG} \right|_{max} K_1 \text{ and } K_2 > \left| \frac{dP_p}{dG} \right|_{max} K_1 \quad (15)$$

The above conditions show that the error tends to zero at least asymptotically. In practice, equilibrium needs to be reached in finite time. The appropriate stability notion in this situation is so-called finite time stability, which is reviewed in Appendix I. It is also demonstrated that $\varepsilon(t)$ attains $\varepsilon = 0$ in finite time [68].

It is worth mentioning that the previous conditions only depend on knowing $\left. \frac{dP_p}{dG} \right|_{max}$, which can be obtained from the P-G curve, and, in particular, from the asymptotic approximation presented below in sub-section III-E. In the subsequent analysis, we consider that the parameters of the MPPT satisfy the above stability conditions. Hence, if $P_{Pref}(t)$ changes and the stability conditions are satisfied, $P_p(t)$ will track the reference $P_{Pref}(t)$. Now it is necessary to determine under what conditions the MPPT increases $P_{Pref}(t)$ until it reaches the MPP.

B) Convergence towards the maximum power point

To analyze the evolution of $P_{Pref}(t)$, the nonlinear function $v(\varepsilon)$ is modified by inserting a hysteresis band while u remains ideal (see Fig. 6).

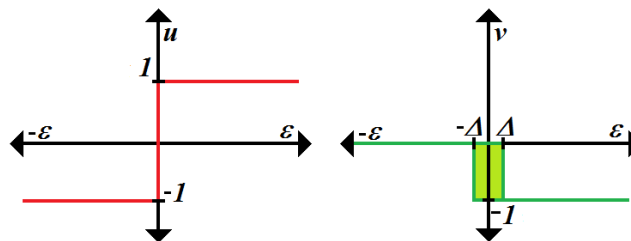


Fig. 6. Switching functions of the proposed MPPT.

At time t_0 , $v = 0$ and $u = 1$. The error increases until it reaches the value Δ at time t_1 (i.e. $\varepsilon(t_1) = \Delta$). At t_1^+ , $v = -1$ and $u = 1$ and the error decreases from Δ to $-\Delta$, which it reaches at time t_3 (i.e. $\varepsilon(t_3) = -\Delta$). But at time t_2 (between instants t_1 and t_3), the error crosses zero and at instant t_2^+ , $u = -1$ and $v = -1$ (see Fig. 7a). At time t_3^+ , $v = 0$ and $u = -1$. The error then increases until it reaches the value Δ , but at time t_4^+ , the error crosses zero and changes the value of u ($u = 1$), with v remaining equal to zero. Then the system returns to the initial configuration $v = 0$ and $u = 1$ and so on. To sum up, the trajectory associated to ε depends on the repeated sequence presented at the bottom of Fig.7b with the associated time

intervals. The resulting waveforms of $P_{p_{ref}}(t)$, $G(t)$, $v(t)$, and $u(t)$ induced by the repeated sequences in the P-G characteristic curve are shown in Fig. 7b. If $P_{p_{ref}}(t_4) > P_{p_{ref}}(t_0)$, after completing a sequence, then $P_{p_{ref}}(t)$ will increase towards the maximum power point.

The dynamical equations describing the motion of $P_{p_{ref}}(t)$ and $G(t)$ for each time interval can be easily calculated using (1)-(4). They are summarized in Table I.

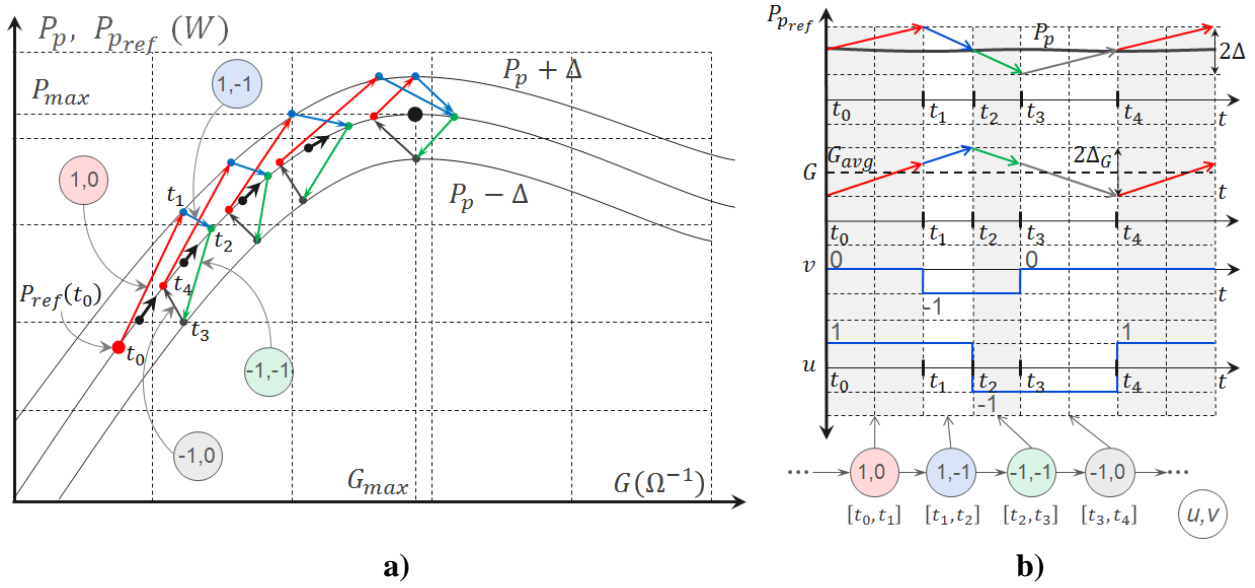


Fig. 7. a) MPP tracking sequences on the P-G curve b) Resulting waveforms related with tracking sequences.

TABLE I
 DERIVATIVES OF $P_{p_{ref}}$ AND G IN THE BASIC MPP TRACKING SEQUENCE

(u,v)	Differential equations describing the dynamic behavior of $P_{p_{ref}}$ and G	
(1,0)	$\left. \frac{dP_{p_{ref}}}{dt} \right _{(1,0)} = K_2 P_p$	$\left. \frac{dP_{p_{ref}}}{dG} \right _{(1,0)} = \frac{K_2}{K_1}$
	$\left. \frac{dG}{dt} \right _{(1,0)} = K_1 P_p$	
(1,-1)	$\left. \frac{dP_{p_{ref}}}{dt} \right _{(1,-1)} = [K_2 - M] P_p$	$\left. \frac{dP_{p_{ref}}}{dG} \right _{(1,-1)} = \frac{K_2 - M}{K_1}$
	$\left. \frac{dG}{dt} \right _{(1,-1)} = K_1 P_p$	

(-1,-1)	$\left. \frac{dP_{p_{ref}}}{dt} \right _{(-1,-1)} = [K_2 - M]P_p$	$\left. \frac{dP_{p_{ref}}}{dG} \right _{(-1,-1)} = \frac{M - K_2}{K_1}$
	$\left. \frac{dG}{dt} \right _{(-1,-1)} = -K_1P_p$	
(-1,0)	$\left. \frac{dP_{p_{ref}}}{dt} \right _{(-1,0)} = K_2P_p$	$\left. \frac{dP_{p_{ref}}}{dG} \right _{(-1,0)} = -\frac{K_2}{K_1}$
	$\left. \frac{dG}{dt} \right _{(-1,0)} = -K_1P_p$	

On the other hand, the time derivative of the error can be expressed as:

$$\frac{d\varepsilon}{dt} = \frac{dP_{p_{ref}}}{dt} - \frac{dP_p}{dt} = \left[\frac{dP_{p_{ref}}}{dG} - \frac{dP_p}{dG} \right] \frac{dG}{dt} \quad (16)$$

Taking into account the expressions in Table I, equation (16) can be particularized for the different states of the basic tracking sequence (see Table II).

TABLE II
MODELING OF THE MPPT POWER ERROR

u,v	Differential equations describing the dynamic behavior of ε
(1,0)	$\left. \frac{d\varepsilon}{dt} \right _{(1,0)} = \left[\frac{K_2}{K_1} - \frac{dP_p}{dG} \right] K_1P_p = \left[K_2 - K_1 \frac{dP_p}{dG} \right] P_p$
(1,-1)	$\left. \frac{d\varepsilon}{dt} \right _{(1,-1)} = \left[\frac{K_2 - M}{K_1} - \frac{dP_p}{dG} \right] K_1P_p = \left[K_2 - M - K_1 \frac{dP_p}{dG} \right] P_p$
(-1,-1)	$\left. \frac{d\varepsilon}{dt} \right _{(-1,-1)} = \left[\frac{M - K_2}{K_1} - \frac{dP_p}{dG} \right] (-K_1P_p) = \left[K_2 - M + K_1 \frac{dP_p}{dG} \right] P_p$
(-1,0)	$\left. \frac{d\varepsilon}{dt} \right _{(-1,0)} = \left[-\frac{K_2}{K_1} - \frac{dP_p}{dG} \right] (-K_1P_p) = \left[K_2 + K_1 \frac{dP_p}{dG} \right] P_p$

From the stability conditions in (15), it can be derived that

$$\left. \frac{d\varepsilon}{dt} \right|_{(1,0)} > 0, \quad \left. \frac{d\varepsilon}{dt} \right|_{(1,-1)} < 0, \quad \left. \frac{d\varepsilon}{dt} \right|_{(-1,-1)} < 0, \quad \left. \frac{d\varepsilon}{dt} \right|_{(-1,0)} > 0 \quad (17)$$

This result is in accordance with the waveform of Fig. 7. If Δ is assumed to be small, P_p and $\frac{dP_p}{dG}$ will not significantly vary within the range of lengths Δ . Consequently, they can be regarded as practically constant in this range. Taking into account the equations describing the motion of ε , the following expressions are deduced:

$$\begin{aligned} t_1 - t_0 &\cong \frac{\Delta}{\left[K_2 - K_1 \frac{dP_p}{dG} \right] P_p}, & t_2 - t_1 &\cong \frac{\Delta}{\left[M - K_2 + K_1 \frac{dP_p}{dG} \right] P_p} \\ t_3 - t_2 &\cong \frac{\Delta}{\left[M - K_2 - K_1 \frac{dP_p}{dG} \right] P_p}, & t_4 - t_3 &\cong \frac{\Delta}{\left[K_2 + K_1 \frac{dP_p}{dG} \right] P_p} \end{aligned} \quad (18)$$

Using the expressions of the time derivatives of the error in Table I, the variation of P_{Pref} can be easily evaluated in the interval $[t_0, t_4]$ as follows:

$$\begin{aligned} P_{Pref}(t_4) &\cong P_{Pref}(t_0) + K_2 P_p(t_1 - t_0) + (K_2 - M) P_p(t_2 - t_1) + (K_2 - M) P_p(t_3 - t_2) \\ &\quad + K_2 P_p(t_4 - t_3) = P_{Pref}(t_0) + K_2 P_p(t_4 - t_0) - M P_p(t_3 - t_1) \end{aligned} \quad (19)$$

After some simple algebraic calculations, we obtain:

$$\begin{aligned} K_2 P_p(t_4 - t_0) - M P_p(t_3 - t_1) &= \Delta \left[\frac{2K_2^2}{K_2^2 - K_1^2 \left(\frac{dP_p}{dG} \right)^2} - \frac{2(M - K_2)^2}{(M - K_2)^2 - K_1^2 \left(\frac{dP_p}{dG} \right)^2} \right] \\ &= \Delta [f(K_2) - f(M - K_2)] \end{aligned} \quad (20)$$

where $f(x)$ is defined by:

$$f(x) = \frac{2x^2}{x^2 - a^2} \quad \text{with } a = K_1 \frac{dP_p}{dG} \quad (21)$$

The derivative of $f(x)$ is given by:

$$\frac{df(x)}{dx} = \frac{4x(x^2 - a^2) - 2x^2(2x)}{(x^2 - a^2)^2} = \frac{-4a^2x}{(x^2 - a^2)^2} < 0 \text{ if } x > 0 \text{ and } x \neq a \quad (22)$$

If $f(K_2) - f(M - K_2) > 0$, this will imply $P_{p_{ref}}(t_4) > P_{p_{ref}}(t_0)$. Since the derivative of f is negative, K_2 and $M - K_2 \neq K_1 \frac{dP_p}{dG}$ from stability conditions, it can be concluded that $f(K_2) - f(M - K_2) > 0$ if and only if $M - K_2 > K_2$, which can also be written as $M > 2K_2$. Adding this inequality to the above stability conditions yields all the constraints that parameters M, K_1 and K_2 must satisfy. They can be summarized as follows:

$$M > 2K_2 \text{ and } K_2 > \left| \frac{dP_p}{dG} \right|_{max} K_1 \quad (23)$$

From the above analysis, $P_{p_{ref}}(t)$ increases until it reaches the vicinity of P_{mp} , where it imposes the condition $P_p \cong P_{mp}$. Then:

$$\frac{dP_{p_{ref}}}{dt} \cong \frac{dP_p}{dt} \cong \frac{dG}{dt} \cong 0 \text{ and therefore } f_1(P_p, u) = 0, f_2(P_p, v) = 0 \quad (24)$$

Hence, from (3) and (4), the average values \bar{u} and \bar{v} of u and v will be given by

$$\bar{v} = -\frac{K_2}{M} > -1 \text{ and } \bar{u} = 0 \quad (25)$$

C) Influence of parameters Δ, M, K_1 and K_2

This sub-section discusses the performance of the proposed algorithm and evaluates the influence of the parameters Δ, M, K_1 and K_2 . The period T_p of the oscillation around the power P_p is equal to $t_4 - t_0$. Then it can be expressed as:

$$T_p = \frac{2K_2\Delta/P_p}{K_2^2 - K_1^2 \left(\frac{dP_p}{dG} \right)^2} + \frac{2(M - K_2)\Delta/P_p}{(M - K_2)^2 - K_1^2 \left(\frac{dP_p}{dG} \right)^2} \quad (26)$$

When the algorithm reaches P_{mp} , then $\frac{dP_p}{dG} \cong \frac{dP_{p_{ref}}}{dG} \cong 0$. Hence,

$$T_p = T_{mp} = \frac{2\Delta M}{K_2(M - K_2)P_{mp}} \quad (27)$$

The associated frequency is given by:

$$f_{mp} = \frac{K_2(M - K_2)P_{mp}}{2\Delta M} \quad (28)$$

where Δ and K_2 are constant.

Considering the constraints $2K_2 < M < \infty$, then $f_{mp} \in \left] \frac{K_2 P_{mp}}{4\Delta}, \frac{K_2 P_{mp}}{2\Delta} \right[$. Hence, the frequency f_{mp} can be controlled by appropriately selecting the parameters Δ, M and K_2 . Now, the amplitude of the fluctuations of the power reference around the maximum point P_{mp} is evaluated. Its determination is illustrated in Fig. 8.

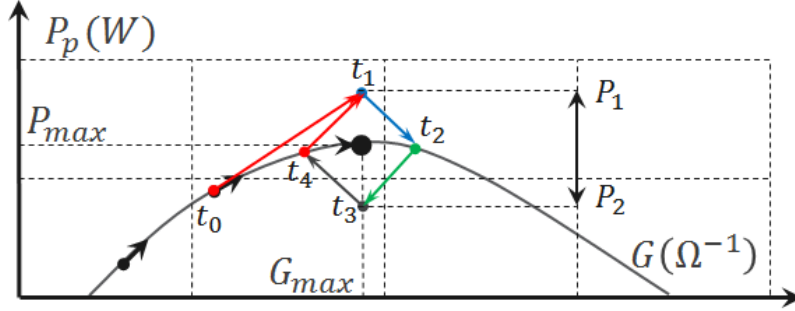


Fig. 8. Determination of the amplitude of power reference and conductance at the maximum power point.

From Table I, the amplitude of the oscillation in the power reference shown in Fig.8 will be given by:

$$\begin{aligned} \Delta P_{Pref} &= P_{Pref}(t_1) - P_{Pref}(t_3) = -(K_2 - M)P_p(t_2 - t_1) - (K_2 - M)P_p(t_3 - t_2) \\ &= (M - K_2)P_p(t_3 - t_1) = \frac{2(M - K_2)^2 \Delta}{(M - K_2)^2 - K_1^2 \left(\frac{dP_p}{dG} \right)^2} \end{aligned} \quad (29)$$

At the maximum power point $\frac{dP_p}{dG} \cong 0$ and, therefore, $\Delta P = P_1 - P_2 = 2\Delta$, as expected. The parameter Δ is the only parameter used to express the amplitude of power fluctuations. Hence, the conductance is constrained to lie in a band of width $\Delta G = G(t_2) - G(t_4)$ given by:

$$\Delta G = K_1 \frac{\Delta M}{\left[M - K_2 - K_1 \frac{dP_p}{dG} \right] \left[K_2 + K_1 \frac{dP_p}{dG} \right]} \quad (30)$$

At the maximum power point, $\frac{dP_p}{dG} \cong 0$, which implies:

$$\Delta G = \frac{K_1 \Delta M}{(M - K_2) K_2} \quad (31)$$

considering the constraints $2K_2 < M < \infty$, then $\Delta G \in \left] \frac{K_1 \Delta}{K_2}, \frac{2 K_1 \Delta}{K_2} \right[$.

It can be concluded that the value of Δ controls the amplitude of the power fluctuations around P_{mp} and that three parameters, namely, M , K_1 and K_2 , can be used to regulate the frequency and the conductance fluctuations around the maximum. From (23) and (31), it can be observed that the smaller K_1 is, the more insensitive the algorithm is to $\left| \frac{dP_p}{dG} \right|_{max}$, and the weaker the effect on the variation of $\Delta G(t)$. Nonetheless, this effect must be sufficient to guarantee that MPPT behaves well.

Moreover, the value of Δ has a significant influence over both static and dynamic performances of the algorithm. A low value of Δ implies high values of tracking efficiency but also high duration of the transient state to reach a new MPP after a sudden change of irradiance. Besides, it is worth mentioning that a value of M broadly satisfying inequality (23), e.g. M between four and ten times higher than K_2 , improves the rapidity and tracking efficiency of the algorithm.

D) Behavior under variations in irradiance

When irradiance is constant, the characteristics of the power of a PV module are represented by a single curve, which is described here as a function of the conductance (P-G). Now, we describe the behavior for variations in irradiance.

Increase in irradiance: Before the change, $P_{pref}(t)$ is at maximum admissible power (for example P_{mp1} in Fig. 9). Due to this abrupt change at t_1 , $P_p(t)$ suffers a discontinuity and the panel characteristic curve suddenly changes. The power of this new curve is higher for all values of G . In this case, we have $\varepsilon(t_1^+) = P_{pref}(t_1^+) - P_p(t_1^+) < 0$. For $t_1^+ > t_1 + \delta$, where δ is positive, we have:

$$\frac{dP_{pref}(t)}{dt} = K_2 P_p(t) > 0 \text{ and } \frac{dG(t)}{dt} = -K_1 P_p(t) < 0 \quad (32)$$

$P_{Pref}(t)$ is increasing and $G(t)$ is decreasing, so $P_p(t)$ is decreasing until it is equal to $P_{Pref}(t)$ at t_2 . From the analysis in the subsections above, $P_{Pref}(t)$ and $P_p(t)$ will move towards the new maximum, which they reach at t_3 (see Fig. 9).

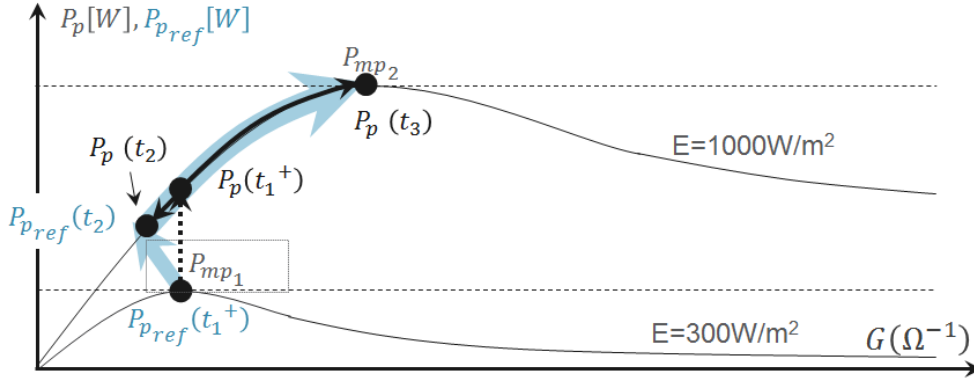


Fig. 9. Trajectories in the plane P-G after a sudden positive change in irradiance.

- **Decreasing irradiance:** With the same notations as before, we have $\varepsilon(t_1^+) = P_{Pref}(t_1^+) - P_p(t_1^+) > 0$. For $t_1^+ > t_1 + \delta$, where δ is positive, we have:

$$\frac{dP_{Pref}(t)}{dt} = (K_2 - M)P_p(t) < 0 \text{ and } \frac{dG(t)}{dt} = K_1P_p(t) > 0 \quad (33)$$

$P_{Pref}(t)$ is decreasing and $G(t)$ is decreasing, so $P_p(t)$ is decreasing until it is equal to $P_{Pref}(t)$ at t_2 . From the analysis in the subsections above, $P_{Pref}(t)$ and $P_p(t)$ will move towards the new maximum, which they reach at t_3 (see Fig. 10).

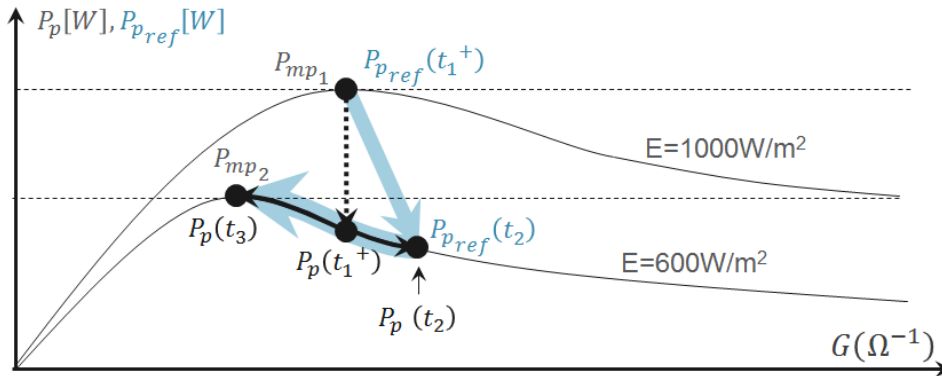


Fig. 10. Trajectories in the plane P-G after a sudden negative change in irradiance.

The analysis of the algorithm is now complete. Even if there are sudden changes in irradiance, the proposed algorithm makes it possible to extract the maximum power of the PV module,

provided that $\left. \frac{dP_p}{dG} \right|_{max}$ is correctly evaluated. The analysis in the subsection below gives the value of $\left. \frac{dP_p}{dG} \right|_{max}$ and makes it possible to select the constants Δ, M, K_1 and K_2 .

E) Approximation of $\left. \frac{dP_p}{dG} \right|_{max}$

The I-V and P-V characteristics of the solar panel are crucial to solve the MPPT problem.

Because of the complexity of the mathematical models that define these characteristics, some methods work with approximations to reduce the complexity of the controller synthesis [69]. In this paragraph, the objective is to asymptotically approximate the I-V and the P-V characteristics of a PV module in order to determine the P-G characteristic curve.

As shown in Fig. 11a, the I-V characteristic curve of a PV module can be approximated by two asymptotes. They are defined using the short circuit current (I_{sc}), the open circuit voltage (V_{oc}) and the voltage corresponding to the maximum power (V_{mp}).

Using this approximation, the I-V characteristic is defined by:

$$i_p(v_p) = \begin{cases} I_{sc} & 0 < v_p < V_{mp} \\ -G_0(v_p - V_{oc}) & V_{mp} < v_p < V_{oc} \end{cases} \quad (34)$$

where $G_0 = I_{sc}/(V_{oc} - V_{mp})$. The P-V characteristic can be deduced by multiplying the previous approximation by v_p . The two asymptotes are transformed into the curves depicted in Fig. 11b. In order to improve the approximation, a third asymptote corresponding to the maximum attainable power (P_{mp}) is introduced. An analytical expression for the derived approximation follows and is given by:

$$p_p(v_p) = \begin{cases} I_{sc} v_p & 0 < v_p < V_1 \\ P_{mp} & V_1 < v_p < V_2 \\ -G_0(v_p^2 - V_{oc} v_p) & V_2 < v_p < V_{oc} \end{cases} \quad (35)$$

where $V_1 = P_{mp}/I_{sc}$ and $V_2 = 0.5V_{oc} + \sqrt{0.25V_{oc}^2 - P_{mp}(V_{oc} - V_{mp})/I_{sc}}$.

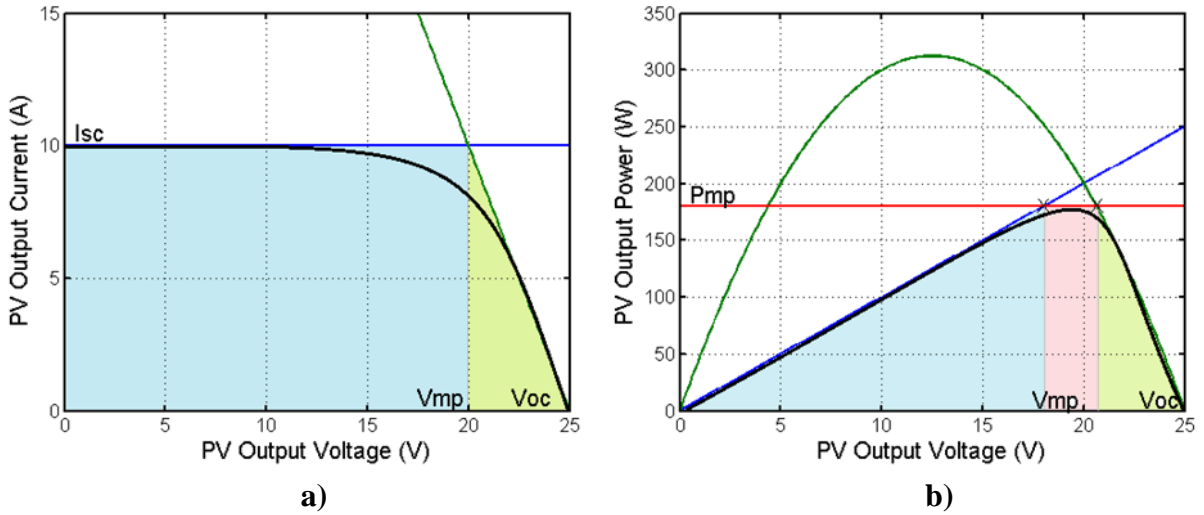


Fig. 11. Asymptotic approach of the characteristic curves of the PV module: a) I-V; b) P-V.

In order to obtain the P-G characteristic, the variable G , which is defined as $G = i_p/v_p$ is introduced in the previous approximation. Since $v_p^2 = p_p/G$, (38) becomes

$$p_p(G) = \begin{cases} G_0^2 V_{oc}^2 \frac{G}{(G + G_0)^2} & 0 < G < G_1 \\ P_{mp} & G_1 < G < G_2 \\ \frac{I_{sc}^2}{G} & G_2 < G < \infty \end{cases} \quad (36)$$

, where $G_2 = I_{sc}^2/P_{mp}$ and $G_1 = \left(G_0^2 V_{oc}^2 \left[1 - \sqrt{1 - 4P_{mp}/(V_{oc}^2 G_0)} \right] - 2G_0 P_{mp} \right) / 2P_{mp}$.

The resulting characteristic is depicted in Fig. 12.

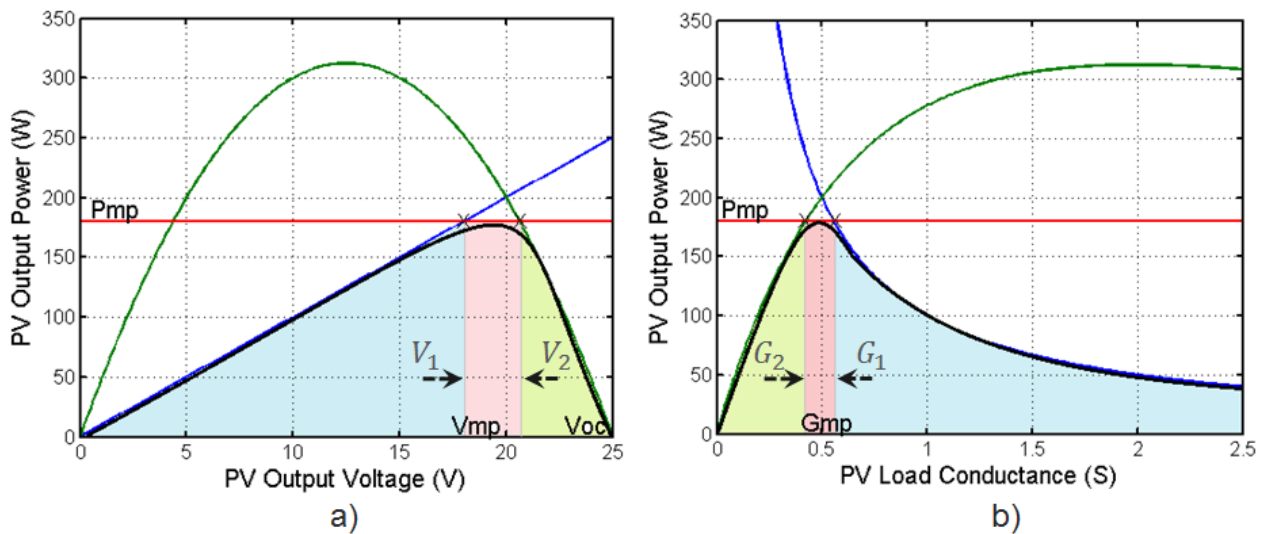


Fig. 12. Asymptotic approach of the characteristic curves of the PV module: a) P-V; b) P-G.

By obtaining the derivatives of (36) and finding their maximum values in their corresponding ranges, it is deduced that the maximum derivative satisfies the following inequality:

$$\frac{dP_p}{dG}_{max} < \max \left\{ \left(\frac{P_{mp}}{I_{sc}} \right)^2, V_{oc}^2 \right\} \quad (37)$$

, where the maximum computed value using (37) is always above the maximum derivative of the real curve.

IV. MICROINVERTER, DC-DC CONVERTER AND INPUT CONDUCTANCE CONTROL

A two-stage microinverter has been selected as the application for the proposed MPPT method. The power stage of the microinverter consists of a quadratic boost converter on the input side and a full-bridge inverter on the output side [70]. As is depicted in Fig. 1c, the output of the DC-DC converter is a power source which supplies the DC link of the microinverter, whose voltage is regulated by the DC-AC stage. This behavior in the quadratic boost converter can be accomplished by using a Sliding Mode controller to force the converter to operate as an SM-LFR. This control uses a given conductance value to induce sliding motions in the input current of the converter. The proposed MPPT tracks the value of the required conductance to permanently extract the maximum power of the PV module. Then, the control of the DC-DC converter uses the conductance computed by the MPPT on the sliding surface given by expression (38).

$$S(x) = i_{in}(t) - v_p(t)G(t) \quad (38)$$

The output voltage of the DC-DC converter does not have a regulation loop acting from the DC-DC converter variables so its value depends on the load. The conductance reference given by the MPPT is quickly imposed on the DC-DC converter by the SM-LFR control and is independent of the load behavior. So, the DC-AC stage can be considered by the DC-DC converter to be a constant voltage load. However, the DC-link voltage contains a double grid frequency component which perturbs the PV module voltage through the reverse audio-susceptibility of the DC-DC converter. Since the paper focuses on the MPPT method, only a general description of the DC-DC

V. SIMULATED AND EXPERIMENTAL RESULTS

In order to verify the theoretical prediction of the MPPT behavior, a set of simulations was implemented in PSIM using the parameters listed in Table III.

TABLE III
 PARAMETERS OF THE SIMULATED PV MODULE AT STANDARD TEST CONDITIONS (STC)
 TEMPERATURE = 25 °C AND IRRADIANCE E = 1000 W/M²

Parameter	Symbol	Value
Open-circuit voltage	V_{oc}	5 V
Short-circuit current	I_{sc}	5 A
Maximum power	P_{mp}	20.5 W
Voltage at P_{mp}	V_{mp}	4.5 V
Current at P_{mp}	I_{mp}	4.5 A
Slope at V_{oc}	$dv/di(V_{oc})$	-0.1 V/A
Series resistance	R_s	0.01 Ω
Shunt resistance	R_{sh}	1000 Ω
Saturation current	I_{so}	4.28×10^{-14} A
Band energy	E_g	1.12 eV
Ideality factor	A	1.2
Temperature coefficient	C_T	0.00325 A/K
Number of cells	N_s	6

As can be seen in Table III, a PV module with values of 5 V in the open circuit voltage and 5 A in the short circuit current was selected to adapt the I-V characteristic to the range values used in a digital implementation. The DC-DC stage was simulated as a controlled current source whose value is defined by the product of the conductance given by the MPPT and the measured voltage of the PV module. A capacitor of 10 μ F was connected in parallel with the module. Based on the shaded parameters in table III and expression (37), the maximum derivative is approximated as $\left| \frac{dP_p}{dG} \right|_{max} = 17$. The parameters of the MPPT were chosen to be $K_1 = 0.2$, $K_2 = 10$, $M = 40$ in order to satisfy the conditions defined by (15) considering $\Delta = 0.1P_{p_{max}} = 2$ for a selected $f_{mp} \approx 40$ Hz .

A. Steady-state of the PV module and MPPT variables

Fig. 14 shows the steady-state waveforms when an average power of 19.36 W is supplied by the PV module. The operation at the maximum power point is confirmed because of the double frequency of the power function. The efficiency of the MPPT operating in steady-state or tracking factor, as calculated in [72]-[74], is given by the following expression:

$$\eta_{MPPT}(t) = \frac{\int_0^t P_{p_actual}(\tau) d\tau}{\int_0^t P_{p_max}(\tau) d\tau} \quad (39)$$

, where P_{actual} and P_{p_max} are the respective measured values of the actual power and the maximum power of a PV module during a time interval of duration t .

All the efficiency values presented in this paper refer only to MPPT performance and consequently do not include the efficiency of the converter. The efficiency of the MPPT is computed as 99.8%. The oscillatory components of the PV module variables have amplitudes of 100 mA (3.4%), 170 mV (4%) and 0.062 W (0.5%).

Fig. 14 shows the trajectory of the power in the P-G plane towards the maximum power point. The power reference enters a limit cycle of rhomboidal type around the MPP when this point is reached by the output power. The steady-state of the MPPT variables shows the relation between the time response and the P-G plane representation. The amplitude of the variations in the conductance is 0.05 S and the amplitude of the variations in the power reference is 4 W.

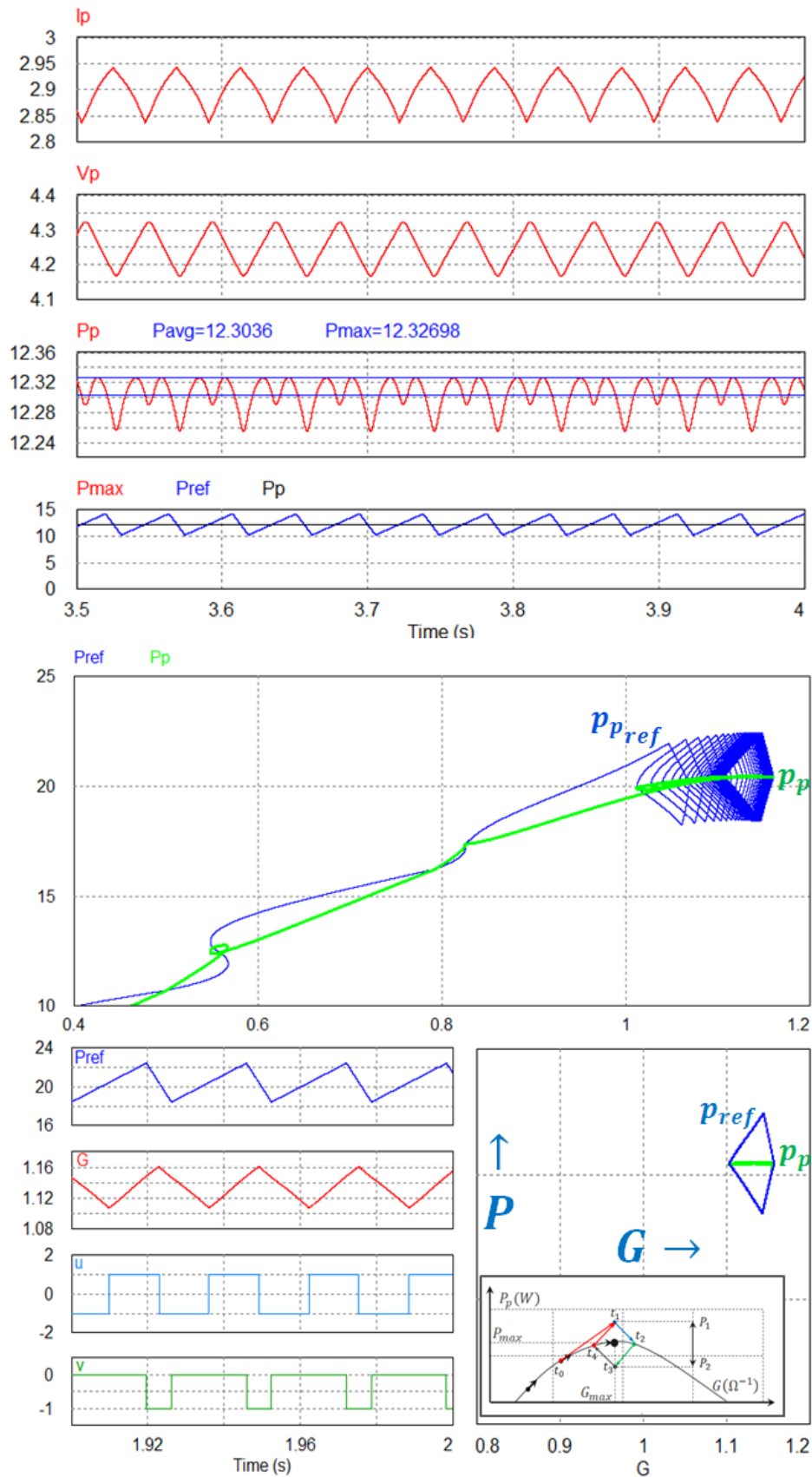


Fig. 14. Detail of the simulated oscillatory components of current, voltage and powers.

B. Dynamic response to changes in the P-V characteristic

Two simulations are used to assess the dynamic response of the MPPT. The first one is the four first waveforms in Fig. 15, which illustrate the effect of variations in irradiance in the Solar Module between 300 and 700 W/m² and vice versa. Each new state lasts for 1 s. The second simulation corresponds to the last four waveforms in the same figure and illustrates the effect of changes between 200 and 1000 W/m² and vice versa using the same time intervals.

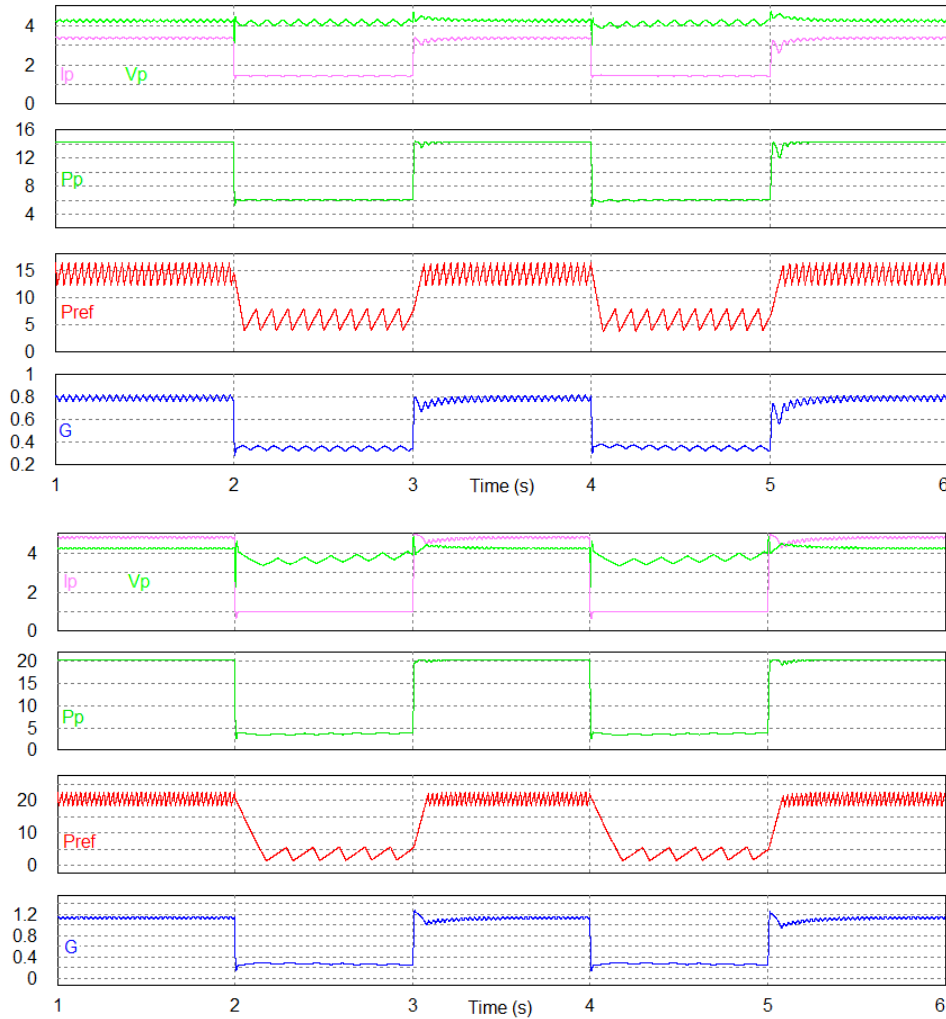


Fig. 15. Simulated results of the dynamic behavior of the algorithm dealing with sudden changes in irradiance between 300 and 700 W/m² and vice versa (top); and between 200 and 1000 W/m² and vice versa (bottom).

As can be noted in both simulations, $P_p(t)$ quickly reaches the maximum power point and shows a smooth transient response when step disturbances are applied to the power. It is also worth noting that in both cases the system behaves similarly and, in general, performs well because maximum power is reached almost instantaneously after a power disturbance penetrates the system.

C. Start-up of the MPPT

In Fig. 16 a simulation of the start-up of the MPPT variables illustrates the transient behavior from the starting point (zero current) to an equilibrium point corresponding to the maximum power. It can be observed that steady state is reached in around 300 ms. Note that the power quickly reaches values in the neighborhood of the maximum power point, thus ensuring appropriate behavior.

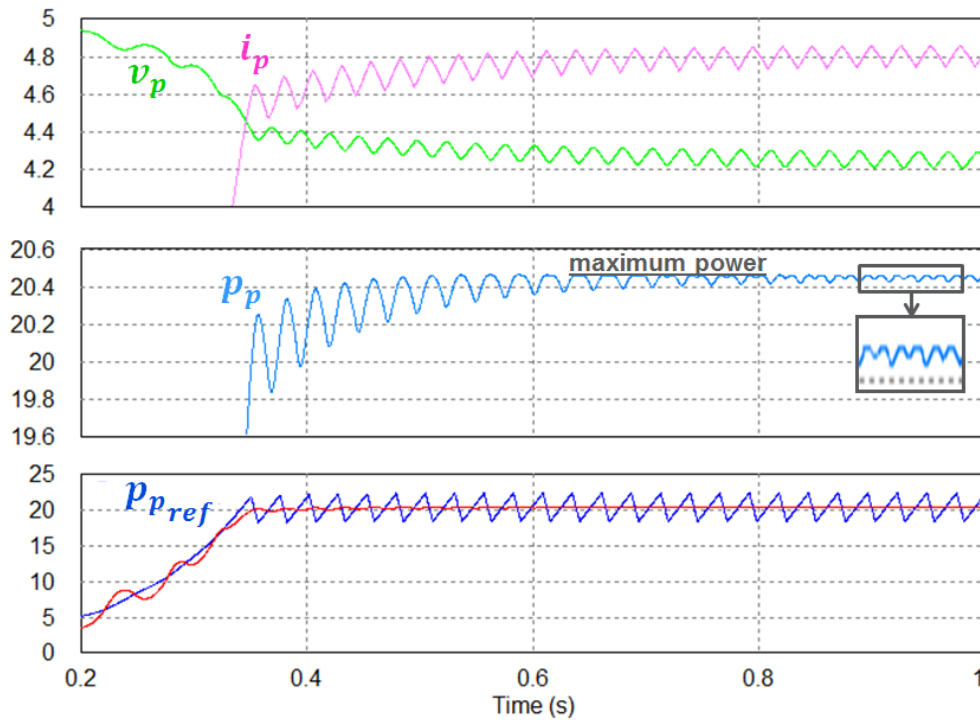


Fig. 16. Response of voltage, current and power during system start-up.

It is important to note that during start-up, both the power reference and the measured power are very close, induced by the control law. Although they do not exhibit the same hysteretic behavior for the maximum power point, both signals oscillate around the MPP. It can be observed in the current and voltage waveforms that the fundamental component of the ripples has the same frequency as the power reference. As a consequence, the ripple in the power of the PV module has a component at the same frequency as the power reference and a component at double frequency, which can be differentiated in terms of the operating point coordinates. When the system operates at the maximum power point, the amplitude of the double frequency component is comparable with the fundamental component (see Fig. 16).

The settling time obtained in the start-up illustrated in Fig. 16 is affected by the low pass filters used to measure the current and voltage required to compute the actual power. It is worth

mentioning that these filters are not a part of the MPPT method and they are only used for the microinverter application. As can be observed in Fig. 17, when the low-pass filters are removed in two different cases, the power of the PV module approaches the amount of power available almost four times faster than in Fig. 16. There is no change in the power reference until the maximum power point has been attained. The time required to reach 90% of the power available is estimated to be less than 80 ms.

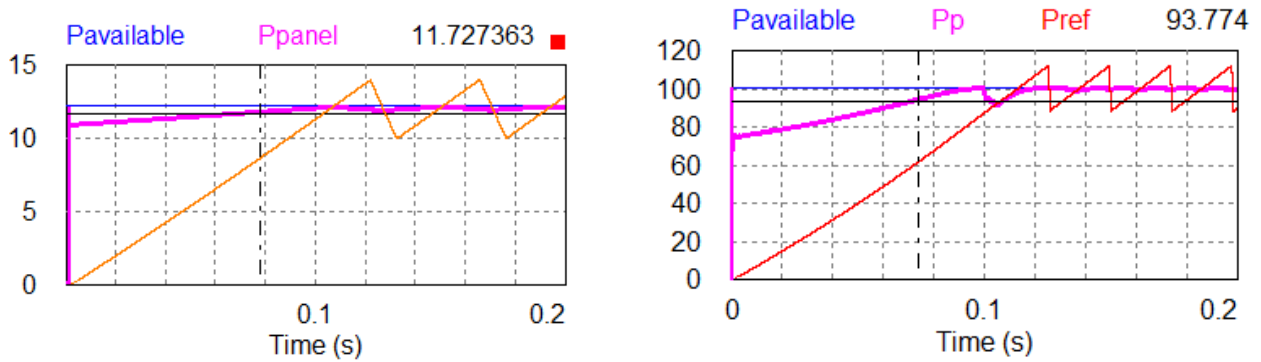


Fig. 17. Power response during system start-up when no low pass filters are used: a) PV module with maximum power of 12 W; and b) PV module with maximum power of 100 W.

D. Prototype and experimental set-up

The MPPT and the SM-LFR control of the DC-DC converter was implemented using a dsPIC30F4011 microcontroller and some analogue electronic circuits. The parameters of the quadratic boost converter are: input inductor (L_1) of 120 μH , intermediate inductor (L_2) of 4.7 mH, input capacitor of 9 μF , intermediate and output capacitors (C_1 and C_2) of 9 μF [71]. The hysteresis is ± 0.5 A. It provides switching frequencies between 130 and 180 kHz for input voltages between 20 and 30 V. A constant sampling frequency of 50 kHz was used in the microcontroller. The serial digital-to-analog (DAC) converter MCP4812 was used to obtain the continuous signals G and $P_{p_{ref}}$. Two digital pins of the micro-controller were used to reproduce the signals of the non-linear functions u and v for the experiments. The set-up for measurements, photovoltaic modules, the converter prototype and the MPPT circuit are shown in Fig. 18. The experimental set-up was constructed at the LAAS-CNRS's ADREAM building in Toulouse, France, a facility that researches renewable energies. The set-up consisted of an E4360A solar panel emulator, an MSO3014 oscilloscope, TCP202 and TCPA300 current probes, an XA3033 power supply, an HP34401A multimeter, an IT8512B electronic load, an MP-160 I-V Curve Tracer, and two BP 585 solar panels whose characteristic parameters are listed in Table IV.

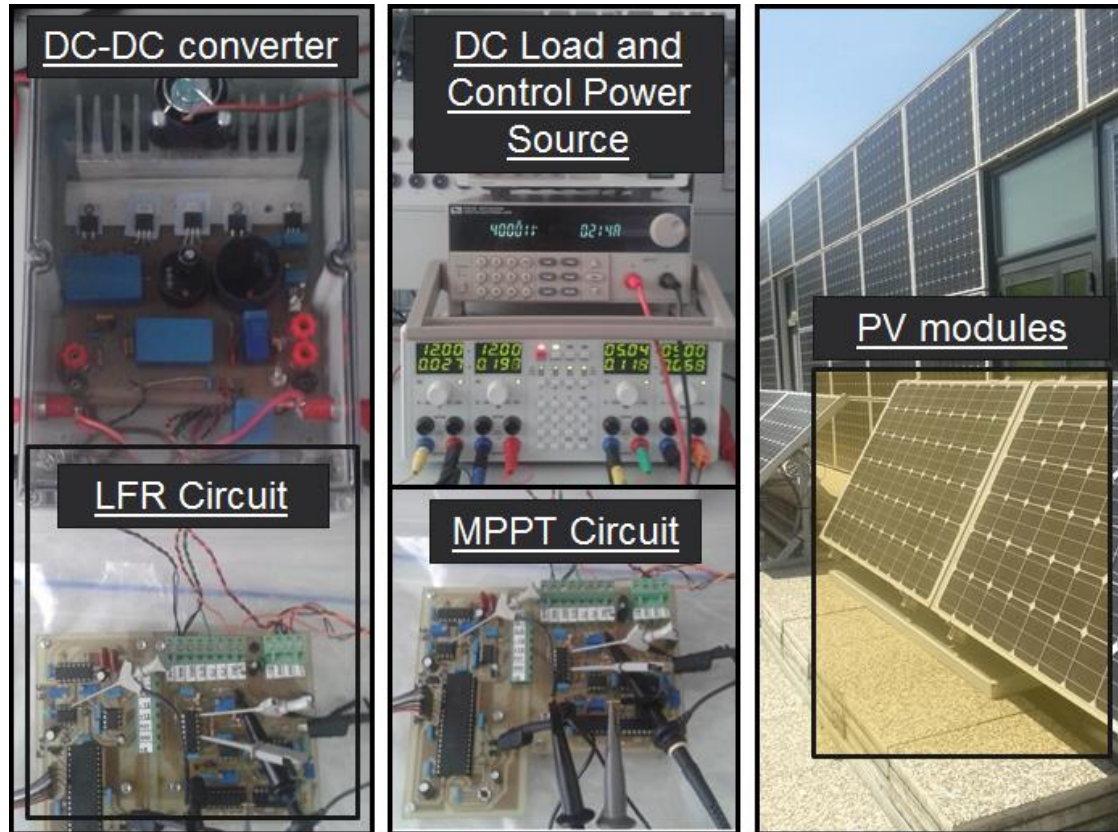


Fig. 18. Converter and MPPT prototype, experimental set-up and panel used in the experiments.

TABLE IV
 PARAMETERS OF THE PV MODULE BP585 AT STANDARD TEST CONDITIONS (STC)
 TEMPERATURE = 25 °C AND IRRADIANCE = 1000 W/M²

Parameter	Symbol	Value
Open-circuit voltage	V_{oc}	22.1 V
Short-circuit current	I_{sc}	5 A
Maximum power	P_{mp}	85 W
Guaranteed minimum P_{mp}	$P_{mp_{min}}$	80.8 W
Voltage at P_{mp}	V_{mp}	18.0 V
Current at P_{mp}	I_{mp}	4.72A

E. Experimental results

Fig. 19a shows the steady-state waveforms when an average power of 91.2 W is extracted from the PV emulator and injected into a voltage load of 400 V through a quadratic boost converter. The PV emulator was configured with an I_{sc} of 4 A and a V_{oc} of 25 V. The maximum derivative for this module was approximated using the asymptotic model to give $\left. \frac{dP_p}{dG} \right|_{max} = 531$. Then, the

parameters of the MPPT were chosen as $K_1 = 0.015$, $K_2 = 10$, $M = 90$, $\Delta \approx 16 \text{ W}$ for a selected $f_{mp} = 25 \text{ Hz}$. The double frequency of the power waveform in comparison with the frequency of the voltage and current waveforms confirms that the system works at the maximum power point (considering a single maximum operational condition). The oscilloscope capture shows the measured power P_p which is compared with the power reference. Using (39) for a maximum power of 92.02 W and an average power of 91.2 W, an MPPT efficiency of 99.1% is obtained. The oscillating components of the PV module variables have amplitudes of 200 mA (5%), 1.6 V (6.6%) and 2.6 W (2.8%), respectively.

The internal signals of the MPPT are also depicted for the maximum power point by comparing the time-based representation with the P-G representation. The four trajectories corresponding to the four structures of the system and the rhombus in steady state are clearly differentiated in Fig. 19b. The waveforms on the left of Fig. 19b show the variation in the conductance and the power reference, and illustrate how the signals u and v induce the motion of the system.

Two tests were performed to assess the dynamic response of the MPPT. In the first test, the I-V characteristic of the panel emulator changed from a first curve with a maximum power of about 95 W to another curve with a maximum power of 65 W and vice versa. Each corresponding I-V characteristic curve is maintained for 500 ms. The waveforms obtained are shown in Fig. 19c. In the second test, the I-V characteristic of the panel emulator changed from a first curve with a maximum power of about 110 W to another curve with a maximum power of 20 W and vice versa. The resulting waveforms are depicted in Fig. 19d. In both tests, the MPPT showed a very rapid response. Furthermore, the panel power $P_p(t)$ reached the vicinity of the maximum value before the power reference, thus improving the general performance and the power harvesting.

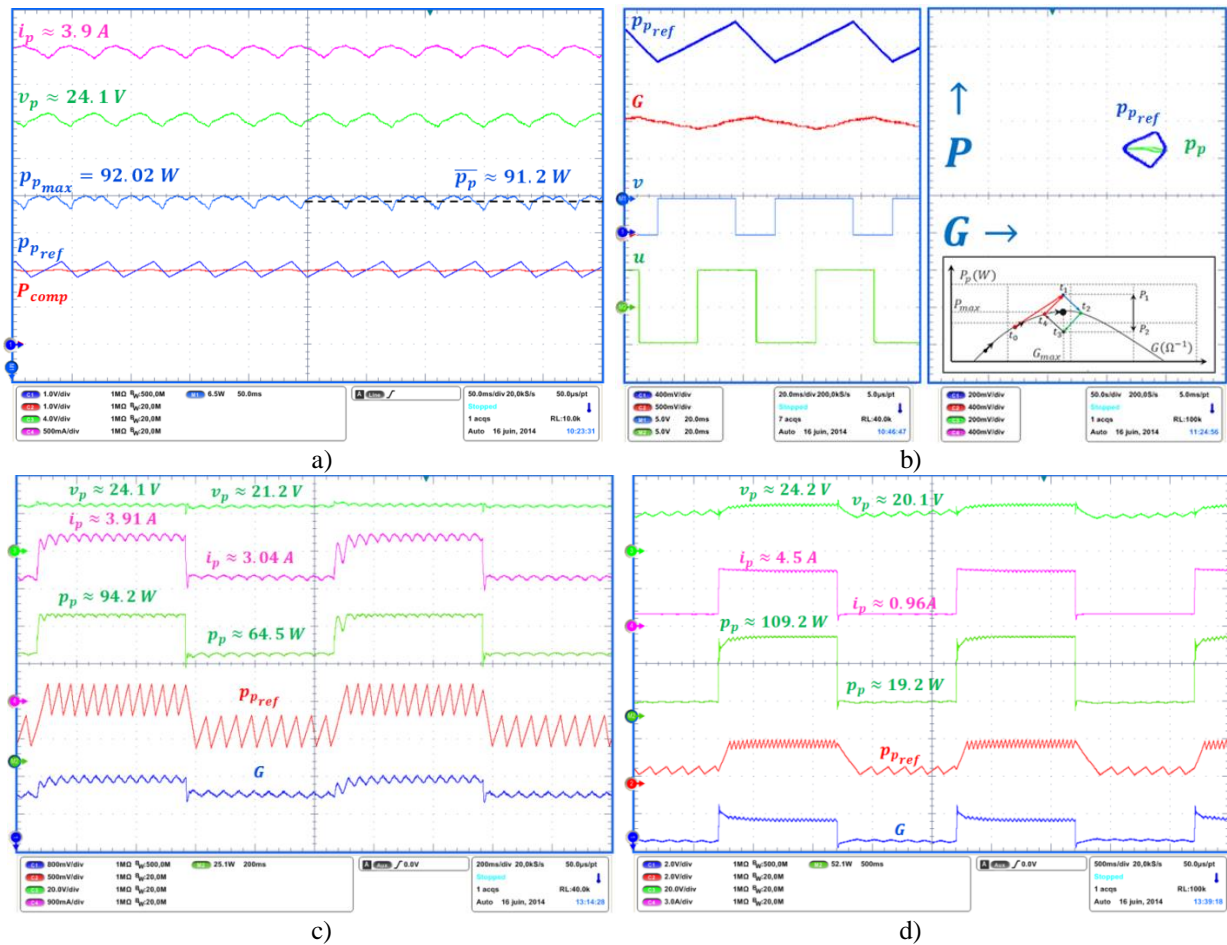


Fig. 19. Experimental results: a) steady-state of the MPPT variables; b) steady- state of the MPPT signals and representation in the P-G plane; c) transient response to 30 W power disturbances; and d) transient response to 80 W power disturbances.

F. MPPT performance operating with the whole microinverter system

The general functionality of the MPPT was also experimentally evaluated using an overall microinverter system connected to the grid and fed by a solar panel. Fig. 20 shows an oscilloscope capture with the system's most representative waveforms. The maximum measured power was 82.24 W while the average power was 81.82 W. The MPPT efficiency computed for this experiment using (39) was 99.49%. The P-V characteristic curve of the panel shown in Fig. 20 was captured with the curve tracer EKO MP-160 and is presented here only for illustrative purposes. The oscilloscope capture shows the power waveform exhibiting the expected double frequency phenomenon at the maximum power point. The power reference and the voltage of the DC bus (400 V) were also measured.

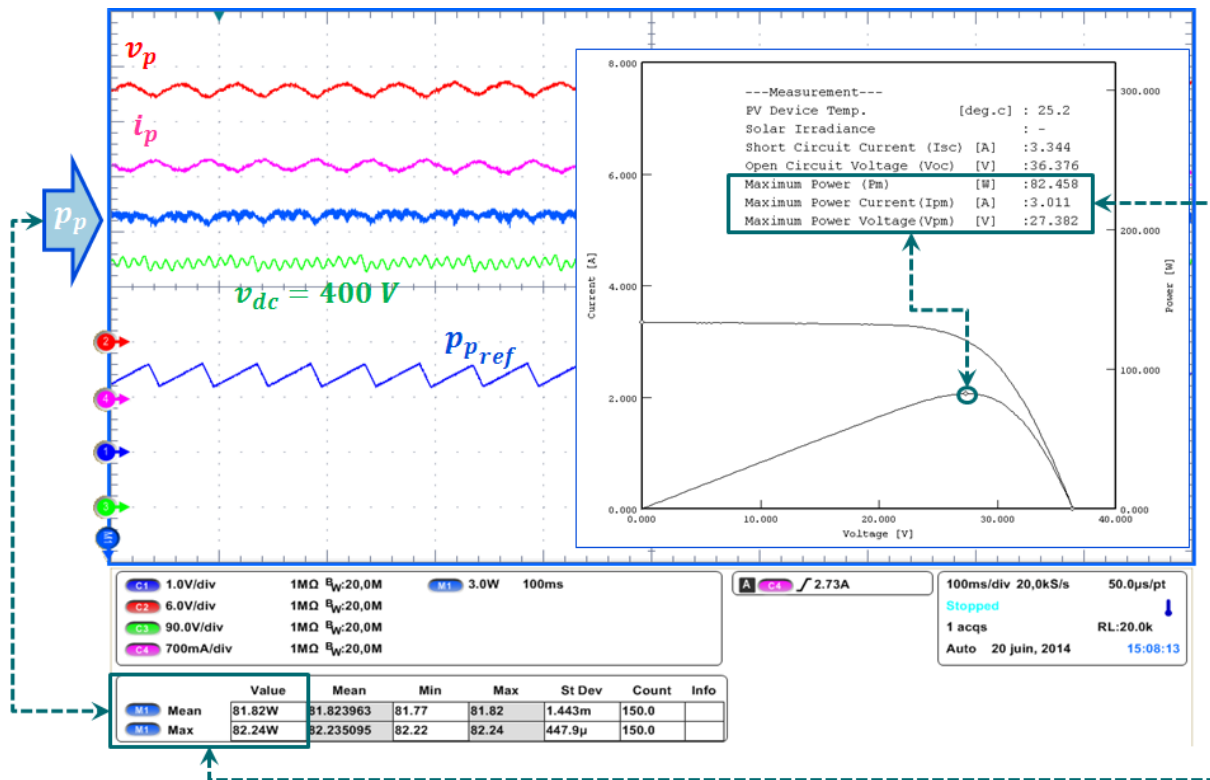


Fig. 20. General validation of the performance of the proposed MPPT.

G. MPPT efficiency for a wide range of power and input voltage

Additional experiments were performed for different levels of voltage and power by measuring the efficiency in three cases, i.e. single solar panel, parallel connection, and series connection of two identical panels. The efficiency results are illustrated in Figs. 21 and 22 in three-dimensional and two-dimensional plots respectively.

It can be observed in Fig. 21 that the efficiency is higher than 99% for a wide range of voltage and power values. This is also verified in Figs. 22 (a) and 22 (b), where the efficiency is plotted as a function of voltage and power respectively. The efficiency increases in a monotonous way in the latter figures from a minimum of 98.2% to a maximum of 99.2%, which correspond respectively to the minimum and maximum values of both voltage and power in the test.

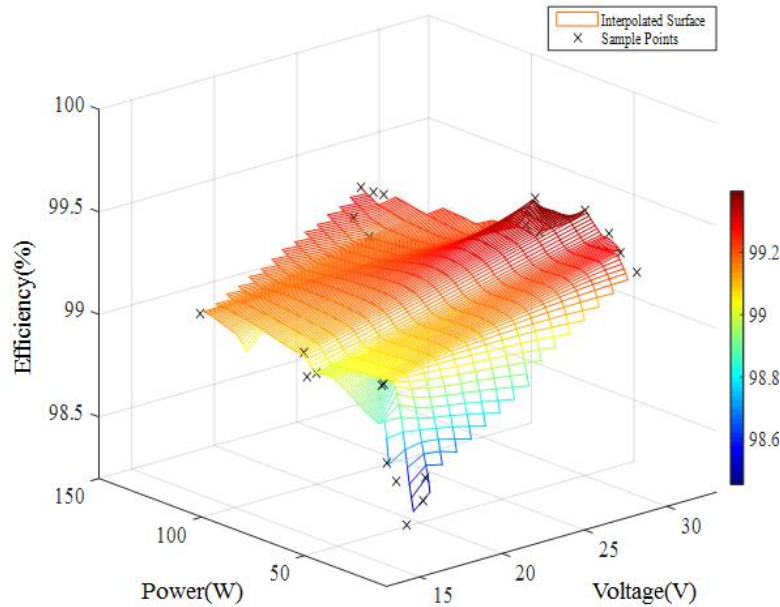


Fig. 21. Tracking efficiency versus voltage and power.

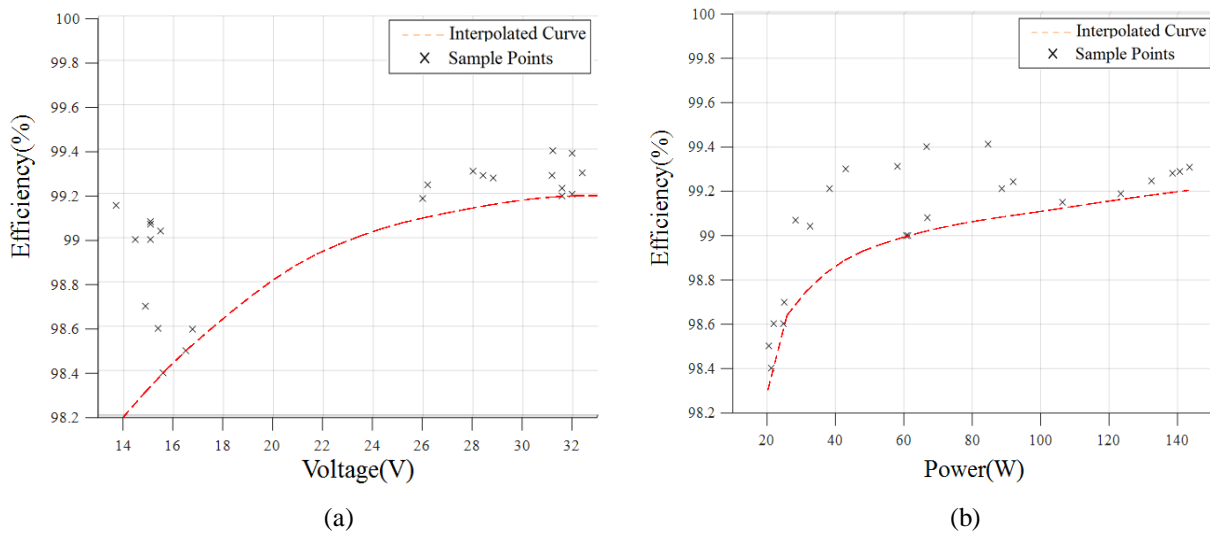


Fig. 22. (a) Tracking efficiency versus voltage (b) Tracking efficiency versus power.

VI. DISCUSSION

In order to make this method comparable to other published methods (i.e. to ensure the same conditions and the optimal set of parameters in each case) a PSIM simulation was then performed. The aim of the simulation is to compare two previously reported ESC methods with the method proposed here (PMPPT) using the converter's input conductance as the manipulated variable in all cases. The first method (FESC) was presented in reference [44] and adapted to a sliding-mode control inner loop of a boost converter in reference [63]. In the application considered in [63], FESC also used the conductance of the converter as the manipulated variable but the MPPT

algorithm was based on a P-V curve and a differentiator had to be used. The second method (SM-ESC) is a variation of the method reported in reference [67]. This variation consists of using the input conductance of the converter instead of the duty cycle as the algorithm output.

In order to compare both steady-state and dynamic performances, a sequence of changes were applied during an interval of operation of one second. All algorithms started from zero initial conditions at $t=0$ operating with 15% of a nominal irradiance of 1000 W/m^2 . After reaching steady state, irradiance disturbances were applied at 0.2, 0.4, 0.6 and 0.8 s which increased and decreased the irradiance in the following sequence $15\% \rightarrow 70\% \rightarrow 45\% \rightarrow 100\% \rightarrow 55\%$ (see Fig. 23). As can be observed, the proposed method not only gives the best response to sudden changes in irradiance in all cases but it also yields the highest MPPT efficiency throughout the interval.

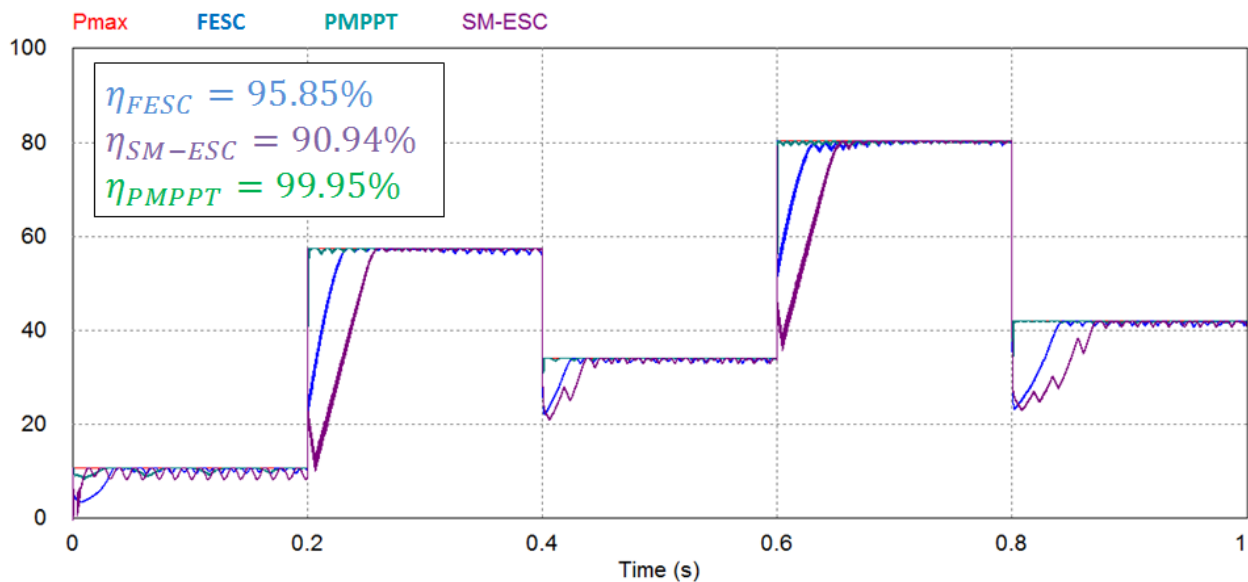


Fig. 23. Simulated results comparing static and dynamic performances of three ESC methods.

To refine the conclusion about the tracking efficiency, a zoom was made for specific values of irradiance for three intervals in steady state. As is depicted in Fig. 24, the proposed method shows that performance was best for low and high irradiance levels, and that it was only slightly less efficient than the SM-ESC method for medium levels (99.82% vs. 99.83%).

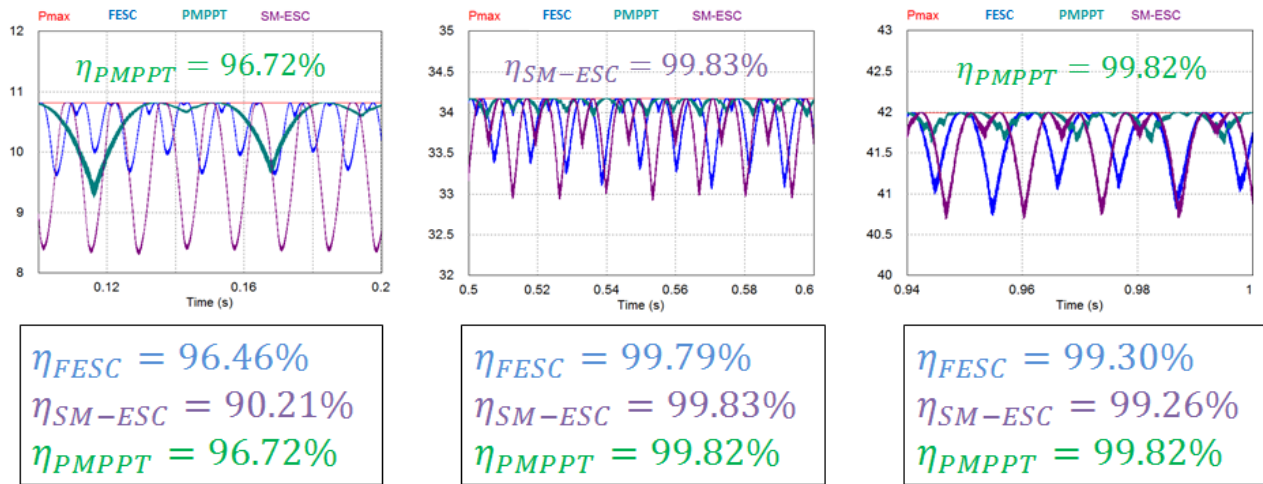


Fig. 24. PSIM simulations showing steady state performance of the three MPPT methods for three different irradiance levels IR: a) IR=150 W/m², b) IR=450 W/m², and c) IR=550 W/m².

To situate the PMPPT in a broader context, we now use the values of the tracking factor in well-known MPPT methods reported in reference [73] for comparative purposes; namely, Gaussian-Arctangent Function-based with Variable Perturbation Frequency (GAF-VPF) (97.8%), Variable step-size Incremental Conductance (VSSINC) (97.32%), Fuzzy (96.50%) and Load-Current Adaptive Step Size and Perturbation Frequency (LCASF) (96.6%). It is commonly accepted that efficiencies above 99% are exceptional; hence, the tracking efficiency of the proposed MPPT is comparable with that of high performance methods. To reinforce this, we processed the measurements for an interval of almost 5 hours. Computing expression (39) using an interval of 17,100 s gave an efficiency of 99.1% (see top of Fig. 25).

The efficiency is minimum for an MPP of 7 W (98.5%), and maximum for an MPP of 61 W (99.6%). This test confirms that the algorithm performs well for a wide range of operational conditions, especially at higher values of irradiance when the amount of power produced is greater. The data were acquired and analyzed with a computational application developed in LabVIEW, two 10-bit channels of a USB-6008 acquisition card, a sensor CAS-15 measuring the current of the PV module, and a simple voltage divider measuring the voltage of the PV module.

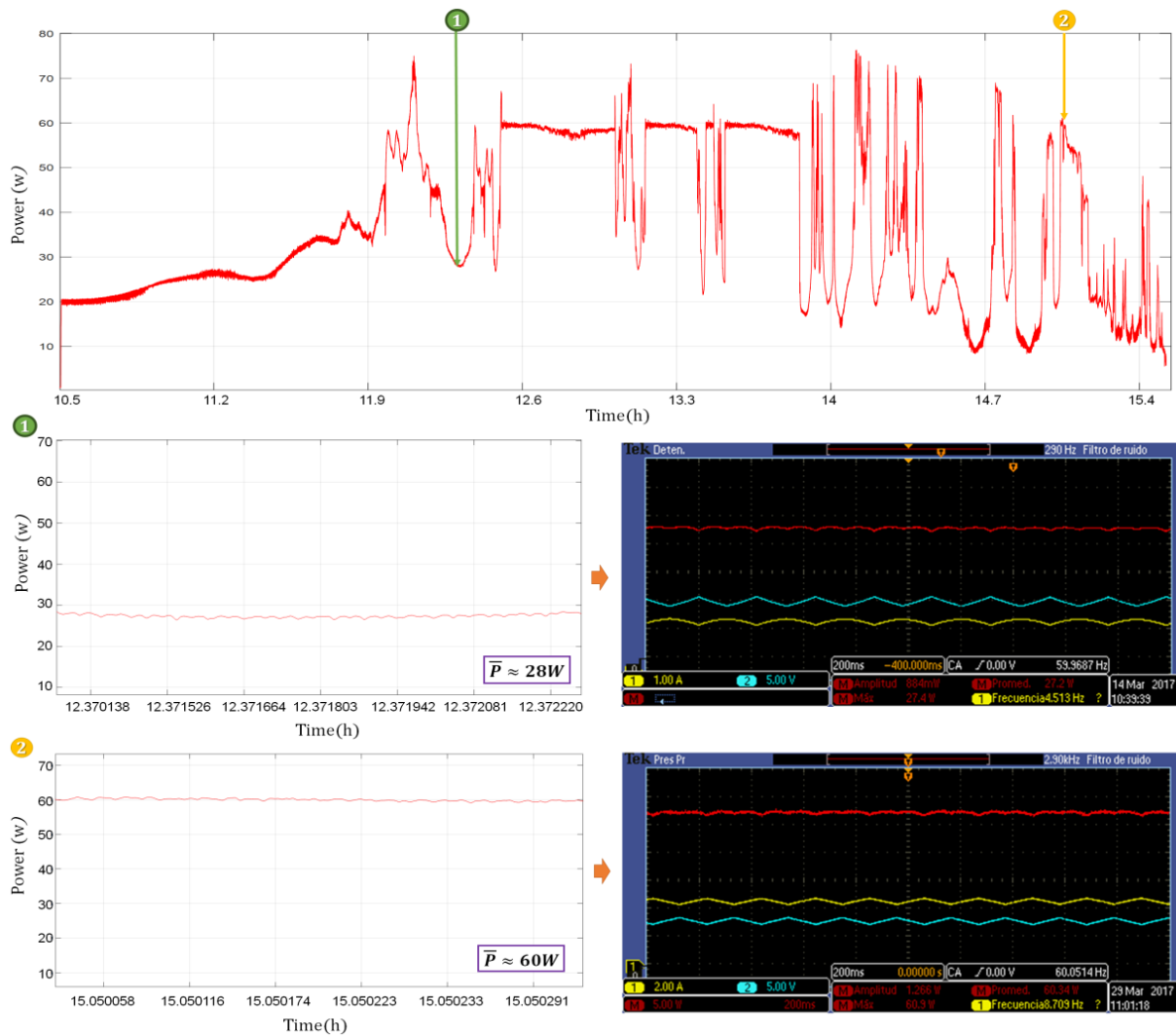


Fig. 25. Experimental results evaluating MPPT dynamic tracking factor for a long-time interval.

The comparative study presented in reference [73] shows that the best dynamic tracking factors reported are lower than 98% (i.e. below the value of 99.6% exhibited by the proposed algorithm). It should be pointed out that the evaluation interval used to calculate the dynamic performance of the proposed MPPT is long and irradiances are below 500 W/m^2 for more than half of the time, which is not in favor of a high tracking efficiency.

The possible ways that the proposed MPPT method can be implemented and its simplicity are also points that can be compared with other existing methods. As is summarized in [6], not all well-known MPPT methods are implementable in both analogue and digital form. Likewise, they are not all equally complex to implement; they are highly dependent on the mathematical functions used. In a clear-cut contrast, the proposed method requires only a few multiplications, sums, integrals, comparisons and gains, and can be implemented in either analogue or digital circuits. In reference [55], which reports a fast and robust MPPT method, analogue implementation is simpler because it requires only seven ICs, and some resistors and capacitors.

In our proposal, nine ICs are required to implement both the MPPT method and the inner current control loop of the LFR; namely, three multipliers, three quad operational amplifiers, two quad comparators and one dual flip-flop. Other methods require derivatives, divisions or even trigonometric functions, which makes the analogue version unrealizable and the digital one much more complex.

This paper has shown how to obtain the rules and guidelines to select an appropriate set of parameters. These parameters are mainly obtained by estimating the maximum derivative of the power with respect to the conductance of a given PV module (based on nominal characteristics). Besides, for a specific PV module used in a MIC, for example, the estimated set of parameters of the MPPT can be tuned so that efficiency and rapidity can be further optimized.

VII. CONCLUSIONS

This paper has discussed an extremum seeking control-based MPPT, which has been studied analytically and described exhaustively. The stability of the control law and the trajectory towards the maximum point have been modeled, studied and validated.

The novelty of the method lies in the fact that a power versus static conductance curve of the PV array is used to accurately track the maximum power point. The MPP is tracked by comparing the instantaneous power of the PV array to a varying power reference generated by the algorithm. The comparison error is used to change the power reference until it reaches the MPP in the P-G curve, and to decrease or increase the conductance at which the PV array is forced to operate. Besides, the instantaneous power determines the amplitude of the nonlinear functions $u(\varepsilon)$ and $v(\varepsilon)$ used in the algorithm, which explains the rapidity with which the tracking mechanism reacts to changes in irradiance.

The method requires only four tuning parameters (K_1 , K_2 , M and Δ), which are selected taking into account the maximum derivative of the power with respect to the conductance. It is also proposed that the derivative for a specific PV module can be evaluated using an asymptotic modelling of the PV module characteristics. As a consequence, the MPPT can be easily tuned to ensure that it operates correctly between 10% and 100% of the nominal power. The method can be implemented using both analogue and digital electronics mainly because of the simplicity of the mathematical functions required.

The high performance of the MPPT was verified with simulation and experimental results. The latter show efficiency values above 98% with a maximum value of 99.6% for a wide range of voltage and power. The MPPT supports sudden changes in the power available and has proved to be robust and reliable. The method has been shown to be comparable with the most efficient maximum power point tracking methods reported in the literature.

ACKNOWLEDGEMENTS

This work was supported by the Spanish Ministerio de Educación e Innovación under projects DPI2016-80491-R (AEI/FEDER, UE) and by the Universidad de Ibagué under project #14-315-INT.

REFERENCES

- [1] B. Subudhi, R. Pradhan, "A Comparative Study on Maximum Power Point Tracking Techniques for Photovoltaic Power Systems," *IEEE Trans. on Sustainable Energy*, vol. 4, no. 1, pp. 89-98, Jan. 2013.
- [2] M.A.G. de Brito, L. Galotto, L.P. Sampaio, G. de Azevedo e Melo, C.A. Canesin, "Evaluation of the Main MPPT Techniques for Photovoltaic Applications," *IEEE Trans. Industrial Electron.*, vol. 60, no. 3, pp. 1156-1167, Mar. 2013.
- [3] D. Sera, L. Mathe, T. Kerekes, S.V. Spataru, R. Teodorescu, "On the Perturb-and-Observe and Incremental Conductance MPPT Methods for PV Systems," *IEEE J. of Photovoltaics*, vol. 3, no. 3, pp. 1070-1078, Jul. 2013.
- [4] S.B. Kjaer, "Evaluation of the "Hill Climbing" and the "Incremental Conductance" Maximum Power Point Trackers for Photovoltaic Power Systems," *IEEE Trans. Energy Conversion*, vol. 27, no. 4, pp. 922-929, Dec. 2012.
- [5] C.B. Salah, M. Ouali, "Comparison of Fuzzy Logic and Neural Network in Maximum Power Point Tracker for PV Systems," *Electric Power System Research*, vol. 81, pp. 43-50, 2011.
- [6] T. Esum, P.L. Chapman, "Comparison of Photovoltaic Array Maximum Power Point Tracking Techniques," *IEEE Trans. Energy Conversion*, vol. 22, no. 2, pp. 439-449, Jun. 2007.
- [7] S. Jain, V. Agarwal, "Comparison of the performance of maximum power point tracking schemes applied to single-stage grid-connected photovoltaic systems," *IET Electric Power Applications*, vol. 1, no. 5, pp. 753-762, Sep. 2007.
- [8] V. Salas, E. Olias, A Barrado, A. Lázaro, "Review of the Maximum Power Point Tracking MPPTs for Stand-Alone Photovoltaic Systems," *Solar Energy Materials & Solar Cells*, vol. 90, pp. 1555-1578, 2006.
- [9] D.P. Hohm and M. E. Ropp, "Comparative study of maximum power point tracking algorithms." *Progress in photovoltaics: Research and Applications*, vol. 11, no. 1, pp. 47-62, Nov. 2002.
- [10] L.V. Hartmann, M.A. Vitorino, M.B.R. Correa, A.M.N. Lima, "Combining Model-Based and Heuristic Techniques for Fast Tracking the Maximum-Power Point of Photovoltaic Systems," *IEEE Trans. Power Electron.*, vol. 28, no. 6, pp. 2875-2885, Jun. 2013.
- [11] K.-J. Lee, R.-Y. Kim, "An Adaptive Maximum Power Point Tracking Scheme Based on a Variable Scaling Factor for Photovoltaic Systems," *IEEE Trans. Energy Conversion*, vol. 27, no. 4, pp. 1002-1008, Dec. 2012.
- [12] A. Chikh and A. "An Optimal Maximum Power Point Tracking Algorithm for PV Systems with Climatic Parameters Estimation," *IEEE Trans. Sustainable Energy*, vol. 6, no.2, pp. 644-652, Apr. 2015.

- [13] Y. Jiang; J.A.A. Qahouq, T.A. Haskew, "Adaptive Step Size With Adaptive-Perturbation-Frequency Digital MPPT Controller for a Single-Sensor Photovoltaic Solar System," *IEEE Trans. Power Electron.*, vol. 28, no. 7, pp. 3195-3205, Jul. 2013.
- [14] K.K. Tse, B.M.T. Ho, H.S.-H. Chung, S.Y. Ron Hui, "A comparative Study of Maximum-Power-Point-Trackers for Photovoltaic Panels Using Switching-Frequency Modulation Scheme," *IEEE Trans. Ind. Electron.*, vol. 51, no. 2, Apr. 2004.
- [15] K. K. Tse, M.T. Ho, H.S.-H. Chung, S.Y.R. Hui, "A novel maximum power point tracker for PV panels using switching frequency modulation," *IEEE Trans. Power Electron.*, vol. 17, no. 6, pp. 980-989, Nov. 2002.
- [16] H.-S. Bae, J.-H. Park, B.-H. Cho, G.-J. Yu, "New MPPT Control Strategy for Two-Stage Grid-Connected Photovoltaic Power Conditioning System," *J. of Power Electron.*, vol. 7, no. 2, pp. 174-180, 2007.
- [17] H.S.-H. Chung, K.K. Tse, S.Y.R. Hui, C. M. Mok, M.T. Ho, "A novel maximum power point tracking technique for solar panels using a SEPIC or Cuk converter," *IEEE Trans. Power Electron.*, vol. 18, no. 3, pp. 717-724, May. 2003.
- [18] M. Veerachary, T. Senjyu, K. Uezato, "Maximum Power Point Tracking of Coupled Inductor Interleaved Boost Converter Supplied PV System," *IEE Proc. Electric Power Applications*, vol. 150, no. 1, pp. 71-80, Jan. 2003.
- [19] K.L. Lian, J.H. Jhang, IS. Tian, "A Maximum Power Point Tracking Method Based on Perturb-and-Observe Combined With Particle Swarm Optimization," *IEEE J. of Photovoltaics*, vol. 4, no. 2, pp. 626-633, Mar. 2014.
- [20] D.C. Jones, R.W. Erickson, "Probabilistic Analysis of a Generalized Perturb and Observe MPPT Featuring Robust Operation in the Presence of Power Curve Traps," *IEEE Trans. Power Electron.*, vol. 28, no. 6, pp. 2912-2926, Jun. 2013.
- [21] A. El Khateb, N.A. Rahim, J. Selvaraj, M.N. Uddin, "Maximum power point tracking of single-ended primary-inductor converter employing a novel optimization technique for proportional-integral-derivative controller," *IET Power Electron.*, vol. 6, no. 6, pp. 1111-1121, Jul. 2013.
- [22] G. Carannante, C. Fraddanno, M. Pagano, L. Piegari, "Experimental Performance of MPPT for Photovoltaic Sources Subject to Inhomogeneous Insolation," *IEEE Trans. Ind. Electron.*, vol. 56, no. 11, pp. 4374-4380, Nov. 2009.
- [23] N. Fermia, G. Petrone, G. Spagnuolo, M. Vitelli, "A technique for Improving P&O MPPT Performances of Double-Stage Grid-Connected Photovoltaic Systems," *IEEE Trans. Ind. Electron.*, vol. 56, no. 11, Nov. 2009.
- [24] D. Sera, R. Teodorescu, J. Hantschel, M. Knoll, "Optimized Maximum Power Point Tracker for Fast-Changing Environmental Conditions," *IEEE Trans. Ind. Electron.*, vol. 55, no. 7, pp. 2629-2637, Jul. 2008.
- [25] R. Faraji, A. Rouholamini, H.R. Naji, R. Fadaeinedjad, M.R. Chavoshian, "FPGA-based real time incremental conductance maximum power point tracking controller for photovoltaic systems," *IET Power Electron.*, vol. 7, no. 5, pp. 1294-1304, May 2014.
- [26] M.A. Elgendy, B. Zahawi, D.J. Atkinson, "Assessment of the Incremental Conductance Maximum Power Point Tracking MPPT," *IEEE Trans. Sustainable Energy*, vol. 4, no. 1, pp. 108-117, Jan. 2013.
- [27] H. Guan-Chyun, H. Hung-I Hsieh, T. Cheng-Yuan, W. Chi-Hao, "Photovoltaic Power-Increment-Aided Incremental-Conductance MPPT With Two-Phased Tracking," *IEEE Trans. Power Electron.*, vol. 28, no. 6, pp. 2895-2911, Jun. 2013.
- [28] G.J. Kish, J.J. Lee, P.W. Lehn, "Modelling and control of photovoltaic panels utilizing the incremental conductance method for maximum power point tracking," *IET Renewable Power Generation*, vol. 6, no. 4, pp. 259-266, Jul. 2012.
- [29] A. Safari, S. Mekhilef, "Simulation and Hardware Implementation of Incremental Conductance MPPT With Direct Control Method Using Cuk Converter," *IEEE Trans. Ind. Electron.*, vol. 58, no. 4, pp. 1154-1161, Apr. 2011.
- [30] Q. Mei, M. Shan; L. Liu, J.M. Guerrero, "A Novel Improved Variable Step-Size Incremental-Resistance MPPT Method for PV Systems," *IEEE Trans. Ind. Electron.*, vol. 58, no. 6, pp. 2427-2434, Jun. 2011.
- [31] A. El Khateb, N. Abd Rahim, J. Selvaraj, M.N. Uddin, "Fuzzy-Logic-Controller-Based SEPIC Converter for Maximum Power Point Tracking," *IEEE Trans. Industry Applications*, vol. 50, no. 4, pp. 2349-2358, Jul. 2014.
- [32] M.AA. Mohd Zainuri, M.A. Mohd Radzi, AC. Soh, N.A. Rahim, "Development of adaptive perturb and observe-fuzzy control maximum power point tracking for photovoltaic boost dc-dc converter," *IET Renewable Power Generation*, vol. 8, no. 2, pp. 183-194, Mar. 2014.

- [33] F. Chekired, C. Larbes, D. Rekioua, F. Haddad, "Implementation of a MPPT Fuzzy Controller for Photovoltaic Synthesis on FPGA Circuit," *Energy Procedia*, vol. 6, pp. 541-549, 2011.
- [34] B.N. Alajmi, K.H. Ahmed, S.J. Finney, B.W. Williams, "Fuzzy-Logic-Control Approach of a Modified Hill-Climbing Method for Maximum Power Point in Microgrid Standalone Photovoltaic System," *IEEE Trans. Power Electron.*, vol. 26, no. 4, pp. 1022-1030, Apr. 2011.
- [35] P.E. Kakosimos, AG. Kladas, S.N. Manias, "Fast Photovoltaic-System Voltage- or Current-Oriented MPPT Employing a Predictive Digital Current-Controlled Converter," *IEEE Trans. Ind. Electron.*, vol. 60, no. 12, pp. 5673-5685, Dec. 2013.
- [36] K. Sundareswaran, S. Peddapati, S. Palani, "Application of random search method for maximum power point tracking in partially shaded photovoltaic systems," *IET Renewable Power Generation*, vol. 8, no. 6, pp. 670-678, Aug. 2014.
- [37] AM. Bazzi and P.T. Krein, "Ripple Correlation Control: An Extremum Seeking Control Perspective for Real-Time Optimization," *IEEE Trans. Power Electron.*, vol. 29, no. 2, pp. 988-995, Feb. 2014.
- [38] J.W. Kimball and P.T. Krein, "Discrete-Time Ripple Correlation Control for Maximum Power Point Tracking," *IEEE Trans. on Power Electron.*, vol. 23, no. 5, pp. 2353-2362, Sep. 2008.
- [39] T. Esram, J.W. Kimball, P.T. Krein, P.L. Chapman and P. Midya, "Dynamic Maximum Power Point Tracking of Photovoltaic Arrays Using Ripple Correlation Control," *IEEE Trans. Power Electron.*, vol. 21, no. 5, pp. 1282-1291, Sep. 2006.
- [40] H. Zazo, R. Leyva and E. del Castillo, "MPPT based on Newton-Like Extremum Seeking Control," in *Proc. IEEE International Symposium on Industrial Electronics (ISIE)*, 2012, pp. 1040-1045.
- [41] X. Li, Y. Li and J.E. Seem, "Maximum Power Point Tracking for Photovoltaic System Using Adaptive Extremum Seeking Control," *IEEE Trans. Control Syst. Technology*, vol. 21, no. 6, pp. 2315-2322, Nov. 2013.
- [42] AM. Bazzi and P.T. Krein, "Concerning Maximum Power Point Tracking for Photovoltaic Optimization Using Ripple-Based Extremum Seeking Control," *IEEE Trans. Power Electron.*, vol. 26, no. 6, pp. 1611-1612, Jun. 2011.
- [43] S.L. Brunton, C.W. Rowley, S.R. Kulkarni and C. Clarkson, "Maximum Power Point Tracking for Photovoltaic Optimization Using Ripple-Based Extremum Seeking Control," *IEEE Trans. Power Electron.*, vol. 25, no. 10, pp. 2531-2540, Oct. 2010.
- [44] R. Leyva, C. Alonso, I. Queinnec, A. Cid-Pastor, D. Lagrange and L. Martinez-Salamero, "MPPT of photovoltaic systems using Extremum - seeking control," *IEEE Trans. Aerospace and Electron. Syst.*, vol. 42, no. 1, pp. 249-258, Jan. 2006.
- [45] C. Cabal, L. Martinez-Salamero, L. Seguier, C. Alonso and F. Guinjoan "Maximum power point tracking based on sliding-mode control for output-series connected converters in photovoltaic systems" *IET Power Electron.*, vol. 7, iss. 4 pp. 914-923, 2014.
- [46] H.-T. Yau, C.-J. Lin and C.-H. Wu, "Sliding Mode Extremum Seeking Control Scheme Based on PSO for Maximum Power Point Tracking in Photovoltaic Systems," *Int. J. of Photoenergy*, vol. 2013, pp. 1-10, 2013.
- [47] E. Bianconi, J. Calvente, R. Giral, E. Mamarelis, G. Petrone, C.A. Ramos-Paja, G. Spagnuolo and M. Vitelli, "A Fast Current-Based MPPT Technique Employing Sliding Mode Control," *IEEE Trans. Ind. Electron.*, vol. 60, no. 3, pp. 1168-1178, Mar. 2013.
- [48] Y. Levron and D. Shmilovitz, "Maximum Power Point Tracking Employing Sliding Mode Control," *IEEE Trans. Circuits and Syst. I: Regular Papers*, vol. 60, no. 3, pp. 724-732, Mar. 2013.
- [49] C.-C. Chu and C.-L. Chen, "Robust maximum power point tracking method for photovoltaic cells: A sliding mode control approach," *Solar Energy*, vol. 83, pp. 1370-1378, 2009.
- [50] J.M.Blanes, F.Javier Toledo, S.Moreno, and A. Garrigós, "In-Site Real-Time Photovoltaic I-V Curves and Maximum Power Point Estimator," *IEEE Trans. Power Electron.*, vol. 28, no. 3, pp. 1234-1240, Mar. 2013.
- [51] G. Spagnuolo, G. Petrone, B. Lehman, C.A. Ramos Paja, Y. Zhao and M.L. Orozco Gutierrez, "Control of Photovoltaic Arrays: Dynamical Reconfiguration for Fighting Mismatched Conditions and Meeting Load Requests," *IEEE Ind. Electron. Magazine*, vol. 9, no. 1, pp. 62-76, Mar. 2015.

- [52] K. Chen, S. Tian, Y. Cheng and L. Bai, "An Improved MPPT Controller for Photovoltaic System Under Partial Shading Condition," *IEEE Trans. Sustainable Energy*, vol. 5, no. 3, pp. 978-985, Jul. 2014.
- [53] S. Moballegh and J. Jiang, "Modeling, Prediction, and Experimental Validations of Power Peaks of PV Arrays Under Partial Shading Conditions," *IEEE Trans. Sustainable Energy*, vol. 5, no. 1, pp. 293-300, Jan. 2014.
- [54] K.-S. Tey and S. Mekhilef, "Modified Incremental Conductance Algorithm for Photovoltaic System under Partial Shading Conditions and Load Variation," *IEEE Trans. Ind. Electron.*, vol. 61, no. 10, pp. 5384-5392, Oct. 2014.
- [55] S. Maity, P.K. Sahu, "Modeling and analysis of a fast and robust module-integrated analog photovoltaic MPP tracker," *IEEE Trans. Power Electron.*, vol. 31, no. 1, pp. 280-291, Jan. 2016.
- [56] T.-K. Soon and S. Mekhilef, "A Fast-Converging MPPT Technique for Photovoltaic System under Fast-Varying Solar Irradiation and Load Resistance," *IEEE Trans. Ind. Informatics*, vol. 11, no. 1, pp. 176-186, Feb. 2015.
- [57] J.S.C.M. Raj and A.E. Jeyakumar, "A Novel Maximum Power Point Tracking Technique for Photovoltaic Module Based on Power Plane Analysis of - Characteristics," *IEEE Trans. Ind. Electron.*, vol. 61, no. 9, pp. 4734-4745, Sept. 2014.
- [58] S.K. Kollimalla and M.K. Mishra, "Variable Perturbation Size Adaptive P&O MPPT for Sudden Changes in Irradiance," *IEEE Trans. Sustainable Energy*, vol. 5, no. 3, pp. 718-728, Jul. 2014.
- [59] S.K. Kollimalla and M.K. Mishra, "A Novel Adaptive P&O MPPT Algorithm Considering Sudden Changes in the Irradiance," *IEEE Trans. Energy Conversion*, vol. 29, no. 3, pp. 602-610, Sept. 2014.
- [60] K. Soon Teya and S. Mekhilef, "Modified Incremental Conductance MPPT for Photovoltaic System under Partial Shading Conditions and Load Variation," *IEEE Trans. Ind. Electron.*, vol. 61, no. 10, pp. 5384-5392, Oct. 2014.
- [61] S. Maity and P. K. Sahu, "Modeling and Analysis of a Fast and Robust Module-Integrated Analog Photovoltaic MPP Tracker," *IEEE Trans. Power Electron.*, vol. 31, no. 1, pp. 280-291, Jan. 2016.
- [62] R. Haroun, A. Cid-Pastor, A. El Aroudi, L. Martinez-Salamero, "Synthesis of Canonical Elements for Power Processing in DC Distribution Systems Using Cascaded Converters and Sliding-Mode Control," *IEEE Trans. Power Electron.*, vol. 29, no. 3, pp. 1366-1381, Mar. 2014.
- [63] A. Cid-Pastor, L. Martinez-Salamero, A. El Aroudi, R. Giral, J. Calvente and R. Leyva, "Synthesis of loss-free resistors based on sliding-mode control and its applications in power processing," *Control Engineering Practice*, vol. 21, no. 5, pp. 689-699, May. 2013.
- [64] R. Haroun, A. El Aroudi, A. Cid-Pastor, G. Garcia, C. Olalla, L. Martinez-Salamero, "Impedance Matching in Photovoltaic Systems Using Cascaded Boost Converters and Sliding-Mode Control," *IEEE Trans. Power Electron.*, vol. 30, no. 6, pp. 3185-3199, June. 2015.
- [65] S. Singer and R.W. Erickson, "Canonical modeling of power processing circuits based on the POPI concept" *IEEE Transactions on Power Electronics*, vol.7,no. 1, pp 37-43, January 1992.
- [66] J.S.C.M. Raj, A.E. Jeyakumar, "A Novel Maximum Power Point Tracking Technique for Photovoltaic Module Based on Power Plane Analysis of - Characteristics," *IEEE Trans. Ind. Electron.*, vol. 61, no. 9, pp. 4734-4745, Sep. 2014.
- [67] AH. Alqahtani, V.I. Utkin, "Self-optimization of photovoltaic system power generation based on sliding mode control," in *Proc. 38th Annual Conf. on IEEE Ind. Electron. Society (IECON)*, 2012, pp. 3468-3474.
- [68] S.P. Bhat and D.S. Bernstein, "Finite-time stability of continuous autonomous systems". *SIAM Journal of Control and Optimization*, vol. 38, no. 3, pp. 751-766, 2000.
- [69] F.-S. Pai, R.-M. Chao, S.H. Ko, T.-S. Lee, "Performance Evaluation of Parabolic Prediction to Maximum Power Point Tracking for PV Array," *IEEE Trans. Sustainable Energy*, vol. 2, no. 1, pp. 60-68, Jan. 2011.
- [70] O. Lopez-Santos, L. Martinez-Salamero, G. Garcia, H. Valderrama-Blavi, "Sliding-mode control of a transformer-less dual-stage grid-connected photovoltaic micro-inverter," in *Proc. 10th Int. Multi-Conf. Systems, Signals & Devices (SSD)*, 2013, pp. 1-6.
- [71] O. Lopez-Santos, L. Martinez-Salamero, G. Garcia, H. Valderrama-Blavi, D. Mercury, "Efficiency analysis of a sliding-mode controlled quadratic boost converter," *IET Power Electron.*, vol. 6, no. 2, pp. 364-373, June 2013.

- [72] D.P. Ohm, & M.E. Ropp, "Comparative study of maximum power point tracking algorithms," *Progress in photovoltaics: Research and Applications*, vol. 11, no. 1, pp. 47-62, Jan. 2003.
- [73] S.M. Reza Tousi, M.H. Moradi, N.S. Basir, & M. Nemati, "A function-based maximum power point tracking method for photovoltaic systems," *IEEE Trans. Power Electron.*, vol. 31, no. 3, Mar. 2016.
- [74] N. Femia, G. Petrone, G. Spagnuolo, & M. Vitelli, *M. Power electronics and control techniques for maximum energy harvesting in photovoltaic systems*. CRC press. 2012.

APPENDIX I

From (1) to (5), we can deduce that:

$$\frac{d\varepsilon}{dt} = \left[\frac{dP_{p_{ref}}}{dG} - \frac{dP_p}{dG} \right] \frac{dG}{dt} = f(\varepsilon)$$

and applying Theorem 4.2 in recalled here for completeness:

Theorem: Suppose there exists a continuous function $V(\varepsilon)$ such that the following conditions hold:

- (i) $V(\varepsilon)$ is positive definite
- (ii) There exist a number $C > 0$, $\alpha \in (0,1)$ and an open neighborhood of the origin such that $V(\varepsilon) + C(V(\varepsilon))^\alpha \leq 0, \varepsilon \neq 0$

Then the origin is a finite-time-stable equilibrium. Moreover, the settling-time function satisfies:

$$T_\varepsilon \leq \frac{1}{C(1-\alpha)} (V(\varepsilon))^{1-\alpha}$$

From (11), (13) and $V(\varepsilon) = \frac{1}{2}\varepsilon^2$ we have:

$$\dot{V}(\varepsilon) = \varepsilon \dot{\varepsilon} = |\varepsilon| P_p \left[-M + K_2 - \frac{dP}{dG} K_1 \right]$$

or:

$$\dot{V}(\varepsilon) = \varepsilon \dot{\varepsilon} = |\varepsilon| P_p \left[-K_2 - \frac{dP_p}{dG} K_1 \right]$$

Depending on the sign of ε . Let us define:

$$C_1 = \left[M - K_2 + K_1 \left| \frac{dP_p}{dG} \right|_{max} \right] P_p(0^+) > 0$$

$$C_2 = \left[K_2 - K_1 \left| \frac{dP_p}{dG} \right|_{max} \right] P_p(0^+) > 0$$

Where positivity follows from conditions in (15). Let $C_3 = \min\{C_1, C_2\}$. From (11) and (13), we can deduce that (remarking that $|\varepsilon| = \sqrt{2[V(\varepsilon)]^{\frac{1}{2}}}$):

$$\dot{V}(\varepsilon) + \sqrt{2}C_3[V(\varepsilon)]^{\frac{1}{2}} = \dot{V}(\varepsilon) + C[V(\varepsilon)]^{\frac{1}{2}} \leq 0, \quad \text{for all } \varepsilon \neq 0$$

From the previous theorem, the error $\varepsilon(t)$ is finite-time stable, meaning that $\varepsilon(t)$ attains $\varepsilon = 0$ in a finite time T_ε satisfying $T_\varepsilon \leq \frac{|\varepsilon(0^+)|}{C_3}$.